

# **Determination of Subsurface Deformations using GPR**

Tatineni Ugesh

A Dissertation Submitted to  
Indian Institute of Technology Hyderabad  
In Partial Fulfillment of the Requirements for  
The Degree of Master of Technology



भारतीय प्रौद्योगिकी संस्थान हैदराबाद  
Indian Institute of Technology Hyderabad

Department of Civil Engineering

July, 2015

## Declaration

I declare that this written submission represents my ideas in my own words, and where others' ideas or words have been included, I have adequately cited and referenced the original sources. I also declare that I have adhered to all principles of academic honesty and integrity and have not misrepresented or fabricated or falsified any idea/data/fact/source in my submission. I understand that any violation of the above will be a cause for disciplinary action by the Institute and can also evoke penal action from the sources that have thus not been properly cited, or from whom proper permission has not been taken when needed.



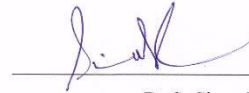
---

Tatineni Ugesh

CE13M1012

## Approval Sheet

This thesis entitled 'Determination of soil deformations using GPR' by Tatineni Ugesh is approved for the degree of Master of Technology from IIT Hyderabad.

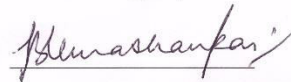


Dr S. Sireesh

Associate professor

Department of Civil Engineering

Indian Institute of Technology, Hyderabad

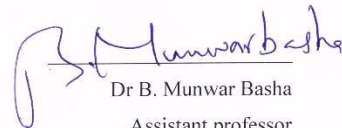


Dr B. Umashankar

Assistant professor

Department of Civil Engineering

Indian Institute of Technology, Hyderabad



Dr B. Munwar Basha

Assistant professor

Department of Civil Engineering

Indian Institute of Technology, Hyderabad



Dr R. Prashanth Kumar

Associate professor

Department of Mechanical & Aerospace Engineering

Indian Institute of Technology, Hyderabad

## **Acknowledgements**

My sincere gratitude to my advisor Dr Sireesh Saride for his continuous support, help, and motivation. I would also like to thank all the faculty members of Civil Engineering Department, IITH.

I am grateful to my family members for their invaluable support.

My heartfelt thanks to Vinay kumar, Raviteja and my classmates Rishitha, Harish and Tejesh.

I would also like to thank Deepti, Vijay Kumar, Pranav and my juniors Uday, Sagar, Ajay, Bhushan and Vinod for being supportive all through days.

I would also like to thank Mallesh and Ravi for helping in the lab.

Dedicated to

**My Family**

## **Abstract**

Non-destructive testing (NDT) is a quality control method which neither damage nor destroy the material being tested. Ground Penetration Radar (GPR) is one of the non-destructive technologies that provides high-resolution information to a greater depths. It works on the principle as reflections occur when there is a change in dielectric properties of two adjacent layers across a soil boundary, or a material interface. GPR is an effective tool for subsurface inspection and quality control, whose applications are very wide and include locating buried objects, detection of voids or cavities, locating steel reinforcement in concrete slabs and also in fields of archaeology and environment. GPR generates radar signal by using Frequency Modulated Continuous Wave (FMCW). These waves can be projected into the ground at a controlled velocity for detection of loose soil pockets. In this study the GPR is first calibrated in three different materials, concrete, clay and sand and the behavior of radargrams is understood. Then the GPR is successfully used in determining the deformations of soil under bridge approach slabs.

# Nomenclature

GPR – Ground Penetrating Radar

$T_x$  – Transmitter signal

$R_x$  – Receiver signal

$R_D$  - Relative Density

ns – Nano Seconds

$t_0$  – Travel time of radar wave

MHz – Mega Hertz

## Contents

Declaration.....	ii
Approval Sheet.....	iii
Acknowledgements.....	iv
Abstract.....	vi
<b>Nomenclature.....</b>	<b>vii</b>
<b>1 Introduction .....</b>	<b>1</b>
1.1 Non-Destructive Testing (NDT) .....	1
1.2 Ground Penetration Radar (GPR) .....	1
1.3 Principle.....	2
1.4 Applications.....	3
1.5 Advantages and Disadvantages of GPR .....	3
1.5.1 Advantages.....	3
1.5.2 Disadvantages.....	5
1.6 Objective .....	5
1.7 Layout .....	5
of .....	
Report .....	
.....	5
<b>2 .....</b>	<b>6</b>
<b>Literature .....</b>	<b>6</b>
<b>review.....</b>	<b>6</b>
2.1 Introduction.....	6
2.2 Background.....	6
<b>3. Calibration.....</b>	<b>11</b>
3.1 Ground .....	
Penetration .....	
Radar .....	
(GPR) .....	
description.....	11
3.1.1 Encoder.....	12
3.1.2 A/D converter.....	12
3.1.3 Monitor/PC .....	12



3.1.4 Control unit.....	13
3.1.5 Antennas.....	13
3.2 Basic working principles.....	13
3.3 GPR antenna frequency description.....	14
3.4 Test procedure.....	14
3.5 Calibration.....	20
3.5.1 Case 1 .....	20
3.5.2 Calculation of Rebar diameter.....	22
3.5.3 Case 2.....	24
3.5.4 Case 3.....	27
<b>4. Determination of Soil Deformations under Bridge Approach Slabs</b> .....	<b>51</b>
4.1 Introduction.....	51
4.2 Pavement Stretch description (from West direction).....	52
4.3 GPR Survey.....	54
4.4 Deformation Modulus of Pavement Sections.....	62
<b>5. Conclusions.....</b>	<b>64</b>
<b>6. References.....</b>	<b>65</b>

# Chapter 1

## Introduction

### 1.1 Non-Destructive Testing (NDT)

Non-destructive testing (NDT) is a quality control method which neither damage nor destroy the material being tested. NDT methods may rely upon use of electromagnetic radiation, sound, and inherent properties of materials to examine samples. NDT is used in a variety of settings that covers a wide range of industrial activity, with new NDT methods and applications, being continuously developed. Non-destructive testing methods are routinely applied in industries where a failure of a component would cause significant hazard or economic loss, such as in transportation, pressure vessels, building structures, piping, and hoisting equipment.

### 1.2 Ground Penetration Radar (GPR)

Ground Penetration Radar (GPR) is one of the non-destructive technologies that provides high resolution information to a greater depths. It works on the principle as reflections occur when there is a change in dielectric properties of two adjacent layers across a soil boundary, or a material interface. GPR is an effective tool for subsurface inspection and quality control, whose applications are very wide and include locating buried objects, detection of voids or cavities, locating steel reinforcement in concrete slabs and also in fields of archaeology and environment. GPR generates radar signal by using Frequency Modulated Continuous Wave (FMCW). These waves can be projected into the ground at a controlled velocity for detection of loose soil pockets.

GPR uses electromagnetic (EM) radio waves. These EM waves are essentially the same as the radio waves that a car antenna receives from a broadcasting radio station. The EM waves are radiated from a transmitter that pulses a signal into the ground. From there the waves are 3 diffracted, refracted, and most importantly reflected. The reflected signals are sent back to the surface where they are measured by a receiver unit, amplified, and digitized by the computer unit that is used to record the measurements.

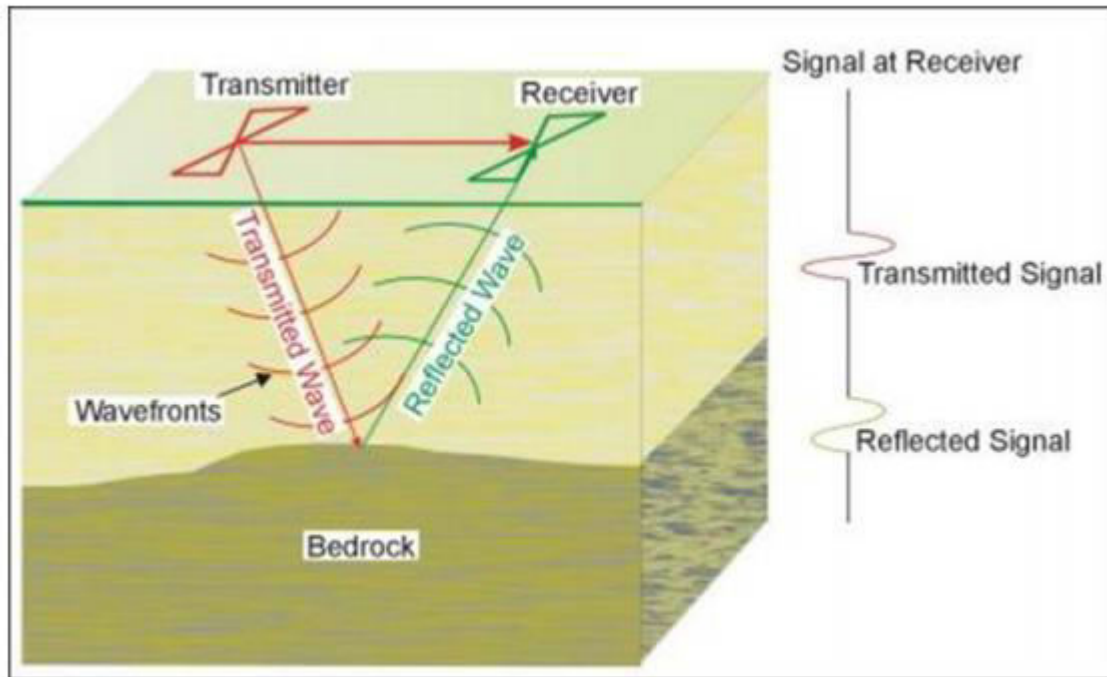


Fig 1.1 Principle of GPR

### 1.3 Principle

Reflection of the wave is due to the subsurface materials having different dielectric properties. When the types of properties of one material are different than that of another above it, a reflected wave will be produced. Each material has its own conductivity level, which produces a certain velocity for the traveling EM waves. Using the reflections and the two way elapsed time of the EM pulse's travel, a cross-sectional reflection profile is created. The profile is often able to be viewed in real time from a computer where the collection of the reflected EM data is taking place. The real time viewing of results allows for possible changes to any parameters that may be adversely affecting the results, including location and equipment settings. Upon further visual interpretation of the results on paper or on a computer screen, a reflection showing continuity throughout the profile may be evidence of a feature of interest. The 4 reflection profile is only part of the puzzle to understanding subsurface phenomena. A further understanding of the geomorphological background of the study area is necessary to complete it. Data collection, while following the same principles, can be achieved in different fashions. The transmitter and receiver are moved along a specified transect in either a stepped or continuous fashion. A step mode of data collection involves both the transmitter and receiver being moved separately at a fixed distance from one another.

## **1.4 Applications**

Ground penetrating radar is a widely accepted field screening technology for characterizing and imaging subsurface conditions. Ground penetration radar (GPR) is most commonly used for locating buried objects such as tanks, pipes, and drums, as well as shallow unexploded ordnance (UXO). It can also be used to map the depth of a shallow water table, identify soil horizons and the bedrock subsurface, and demarcate trench boundaries. It is also used to delineate the physical integrity of manmade structures, such as slurry walls and permeable reactive barrier walls. GPR can also detect plastic, glass, concrete, or wood. Military applications of ground-penetrating radar include detection of unexploded ordnance and detecting tunnels. In military applications and other common GPR applications, practitioners often use GPR in conjunction with other available geophysical techniques such as electrical resistivity and electromagnetic induction methods.

## **1.5 Advantages and Disadvantages of GPR**

### **1.5.1 Advantages**

#### **Comprehensive Geophysical Surveying**

Compared to other geophysical surveying methods, GPR provides the broadest range of geological feature detection; including glaciers, sediment thickness, bedrock, fractures, faults, groundwater, voids and sinkholes.

#### **High Resolution 3D Imaging**

Highly accurate 3D imaging is possible with GPR and the increasing necessity for detailed three-dimensional (3D) resolution of shallow depth structures such as buried utilities and archeological features make GPR acquisition one of the most important remote sensing methods. Equally, the advantages of mapping geological features where high horizontal and vertical resolution is a growing requirement for geoscientists.

#### **Superior Data Density, Quality and Accuracy**

GPR offers the highest resolution of the subsurface compared to any competing geophysical surveying technologies, including seismic methods, transient electromagnetic (EM), electrical techniques and magnetic techniques. Through the selection of antenna frequency, resolution of the data can be increased or decrease to match the requirements of the application. For deep geophysical surveying, GPR is capable

of penetrations up to 30-95 feet deep with accuracy of 0.5 to 3 feet or in the case of shallow pavement assessment accuracy of 3-5% are achievable for asphalt pavement thickness measurement, even when that data is being collected at speeds of over 50mph.

### **Super-Fast Data Acquisition with Wide Coverage**

High speed data acquisition is one of the most attractive advantages of GPR resulting in obvious business benefits of reduced survey costs as well as the reduction and often elimination of association costs of restricting access of other commercial operations to the survey area. In favorable conditions a survey area of a football field can be measured in one day and fully processed in the next. When towed or carried on a vehicle, data can be collected continuously at highway speeds (>55mph).

### **Simple Instrumentation Setup and Portability**

An important advantage of GPR survey technique is that no physical contact between the transmitter and receiver antenna and the subsoil is necessary. This is in contrast to other technique such as seismic where extensive equipment location planning and physical installation is required. With GPR the transmitter and receiver antenna can be place on a cart or carried over the survey area with data acquisition occurring immediately - requiring only one person for the entire data collection process.

### **Depth Information Acquisition and Soil Profiles**

GPR can also provide accurate depth information, something that can be only crudely estimated with other geophysical methods. A major advantage of GPR is that it records vertical soil profiles in detail, rather than generating only horizontal plan maps as in the case of conductivity and magnetometry methods.

### **Deep Penetration with High Resolution**

With favorable soil conditions, GPR is capable of penetrations up to 30-95 feet deep with accuracy of 0.5 to 3 feet. Much greater survey deeps can be achieved by combining GPR with borehole investigations.

### **GPS Compatibility**

The integration of GPS with GPR provides accurate determination of the measurement location while the survey is in progress thereby eliminating the need to mark off a well-defined grid on the survey site and allowing rapid geophysical survey data collection over large areas.

## **Complements other Geophysical Methods**

Due to survey site and soil composition, GPR data interpretation can be ambiguous and it may be desirable to acquire and integrate data from one or more other geophysical methods such as ER to determine the subsurface structure. GPR data is highly compatible with these other geophysical methods and the ability to image the same subsurface with another geophysical method and complement the GPR data can drastically reduce the uncertainty in the interpretation of geophysical data.

## **Non-Destructive and Non-intrusive**

GPR has the benefit of being both non-destructive and non-intrusive. When maintaining access to the survey area is a priority, the benefits of GPR's rapid unobtrusive data collection is a major advantage over other geophysical methods and will likely become a critical consideration in determining what method to deploy.

### **1.5.2 Disadvantages**

Depth of penetration (typically 1 to 15 meters) is less than direct current (DC) resistivity and electromagnetic (EM) methods, and is further reduced in moist and/or clayey soils and soils with high electrical conductivity. Penetration in clays and in materials having high moisture is sometimes less than 1 meter. The GPR method is sensitive to noise—i.e., interference caused by various geologic and cultural factors. For example, boulders, animal burrows, tree roots, and other phenomena can cause unwanted reflections or scattering. Cultural sources of noise can include reflections from nearby vehicles, buildings, fences, power lines, and trees. Electromagnetic transmissions from cellular telephones, two-way radios, television, and radio and microwave transmitters may also cause noise on GPR records. Shielded antennae are used to limit these types of reflections. The bulkiness of equipment can limit use in rough terrain. Unprocessed images require processing, as they provide only approximate shapes and depths

## **1.6 Objectives**

1. To determine reinforcement details such as spacing, diameter of rebar, thickness of slab etc.
2. To understand the working of GPR by burring few objects at known location and at known depth by analyzing the radar grams obtained
3. To determine density changes and soil deformation analyzing radar grams.

## **1.7 Layout of Report**

Within the content of the research, the report is structured in the following main parts:

Chapter 1 briefly describes about the NDT technology, GPR, its principle of working, application, advantages and limitations, objective of the project.

Chapter 2 deals with the literature related to the main research. This is aimed to provide the basic knowledge, which is required for the analysis of the research as well as for the interpretation of the results.

Chapter 3 deals with the equipment description and the calibration part of the GPR.

Chapter 4 deals with the real time survey of determining the soil deformations under Bridge approach slabs.

Chapter 5 deals with the conclusions drawn from the study.

# Chapter 2

## Literature review

### 2.1 Introduction

Ground Penetration Radar (GPR) is one of the non-destructive technologies that provides high-resolution information to a greater depths. It works on the principle as reflections occur when there is a change in dielectric properties of two adjacent layers across a soil boundary, or a material interface. Its applications are getting wide as in the fields such as Archaeology, Environment management, Architecture, mineral prospecting etc. In the field of civil engineering various researchers have worked on GPR and have proposed it to be a very effective non-destructive technique for identifying unknown objects lying underground and also in assessment of pavement condition.

### 2.2 Background

Xian-Qi et al. (2009) have worked on GPR and proposed its various application in the field of concrete slab. Location of reinforcing bars is an important and popular application that has received particular attention with emphasis on the effects of bar size, spacing and depth upon ability to detect individual bars.

Stolte and Nick (1994) investigated the relationship between cylinder radius and hyperbola eccentricity for the purpose of migration, while Olhoeft (2000) attempts in to derive radius information from the curvature of the hyperbola apex with human intervention. Al-Nuaimy et al. (2000) presented one model relates the two-way travel time  $t$  to the horizontal position  $x$  and the velocity of propagation  $v$ . But this model relies on the assumption that the hyperbolic signatures, result from point reflectors, and hence the radius is assumed to be zero. Using this model to characterize the signatures of such targets leads to erroneous information.

S. Shihab and W. Al-Nuaimy (2005) developed a more generalized equation that takes into account the possibility of a finite radius  $R$ . This allows for cylinders of arbitrary radii to be detected and characterized uniquely from a single radargram as shown in Figure 2.1.



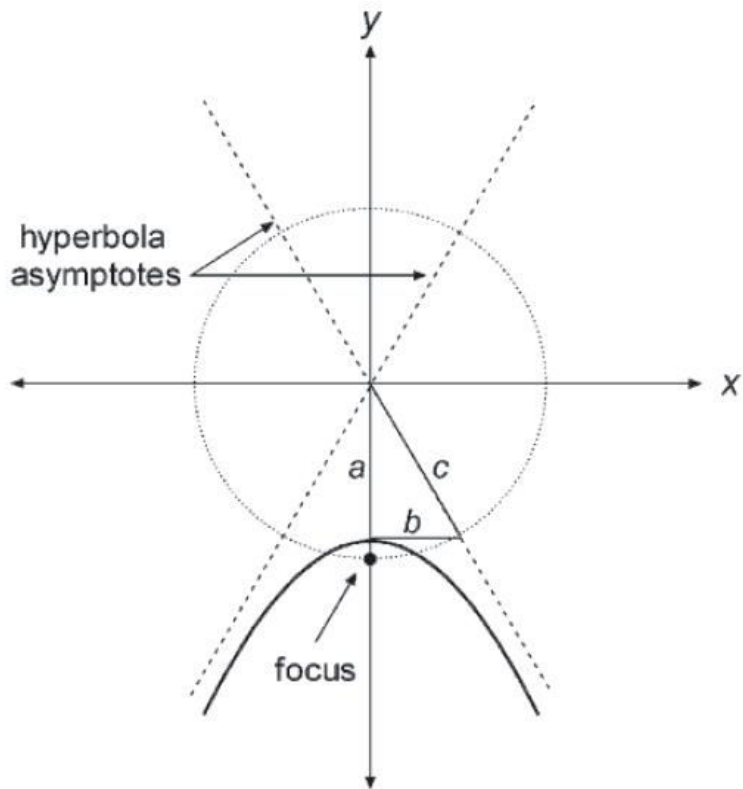


**Fig. 2.1:** Generalized Hyperbola with its asymptotes

S. Shihab also established the following relation between  $R$  and the general hyperbola with its asymptotes  $a$  and  $b$ .

$$a = t_0 + \frac{2R}{v} \dots\dots\dots(1)$$

$$b = \frac{v}{2} \left( t_0 + \frac{2R}{v} \right) \dots\dots\dots(2)$$

$a$ ,  $b$ ,  $t_0$ ,  $v$  are obtained as a result of the fitting process and  $R$  can be calculate from either equation. The fitting technique is applied on a variety of real hyperbolic signatures that are collected from a controlled test site, the results indicate this technique is fully capable of successfully estimating the depth and radius to within 10%, which validates the method.

Chen and Wimsatt (2009) have used a 400 MHz ground-coupled penetrating radar (GCPR) to characterize the subsurface conditions of three roadway pavements. They have successfully demonstrated that the GCPR is able to identify anomalies and void locations. GCPR was used in three projects to identify anomalies under roadway pavements. They have found that presence of moisture under pavement has a significant impact on GCPR signals and causes the dielectric properties to increase substantially with increased water intrusion. They have proposed a formula to calculate the thickness of asphalt layer using the speed of light, two way travel time of signal and dielectric constant. The dielectric constants proposed by them are given in the Table 2.1.

**Table 2.1.** Dielectric constants of few materials

<b>Material</b>	<b>Dielectric constant</b>
Air	1
Granite	9
Limestone	6
Sandstone	4
Dry sand	4 to 6
Wet sand	30
Dry clay	8
Wet clay	33
Asphalt	3 to 6
Concrete	9 to 12
Water	81
Metal	10000

Sun F. Shih et al. (1986) have worked on GPR to investigate the depth of ground water-table in coarse-textured soils using 120MHz antenna and 300MHz antenna. They have conducted separate studies at different localities and proposed that the coefficient of determination,  $r^2$ , between the observed water table and that from radar profile was 0.90.

Sun F. Shih et al. (1994) found the GPR application in assessing a salt affected area. They have used a 120 MHz antenna to assess the salt affected area and the threshold value for GPR penetration was adopted as  $2\text{ds m}^{-1}$  to delineate the salt affected area. However the quantification of amount of salt content was not done.

George Morcouc et al. (2010) have used a 1.6 MHz antenna and have conducted several laboratory and field experiments in determining the concrete pavement thickness. They have also investigated the effect of concrete age on GPR thickness measurement accuracy.

Sandro Colagrande et al. (2011) have used GPR in assessing the Flexible road pavement degradation. They have used 1600 MHz and 600 MHz antennas in studying the degraded road pavements behavior built in cutting sections.

Leucci and Negri (2006) showed the feasibility of GPR methodology in an urban area to locate the buried archaeological structures or monuments. The tests showed that with the help of a 3-D data, the idea of buried objects would be clearer.

According to Maser (2000), GPR is an excellent tool for locating changes in the pavement structure and are clearly visible in the graphic display of the radar data. GPR can be used for pavement characterisation along with the pavement thickness measurement and also to determine the moisture within the asphalt pavement, which no other practical technique can measure.

In the present research based on all the understanding and application of previous works the GPR has been calibrated in three different cases identifying the known buried objects and then the GPR technique have been used in determining the soil deformations under bridge approach slab.

# Chapter 3

## Calibration

### 3.1 Ground Penetration Radar (GPR) description

The first step in choosing a GPR system is to understand the main components of the system. A typical GPR system is comprised of five main components including control unit, antenna, monitor, electronics (AC/DC converter) and encoder as shown in Figures 3.1 and 3.2 that interface and communicate with each other depending on their respective functions. The physical location of each of these components depends on the system and application, and in some cases two or more components may be combined in the same physical unit.

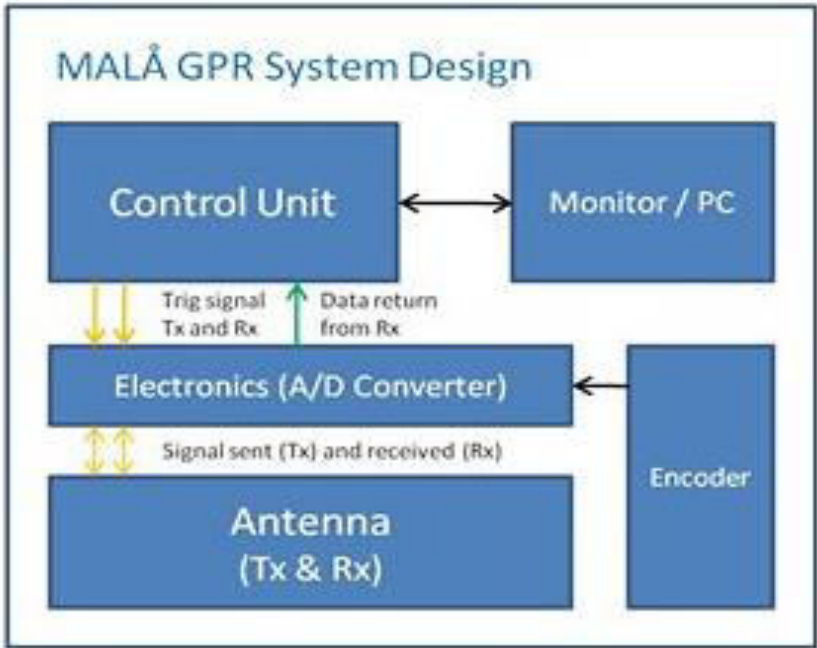


**Fig 3.1:** Typical layout of GPR Equipment

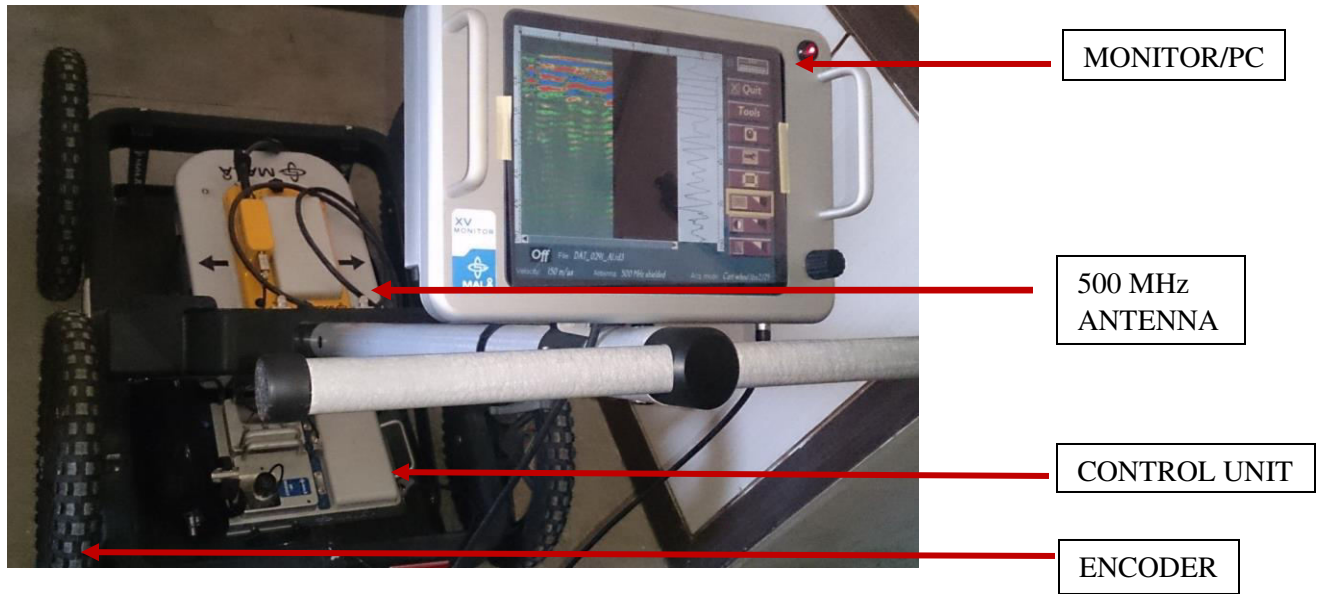


**Fig.3.2:** GPR set-up image with its components

### 3.1.1 Encoder

The Encoder is generally a mechanical device, such as a wheel, that is used to measure the distance along the target area and initiates a triggering pulse for the radar signal at predetermined distances. In some cases, a global positioning system (GPS) is used in the Encoder to determine the location and distance for triggering.

### 3.1.2 A/D converter

The A/D Converter forms the interface between the Antennas and the Control Unit converting signals from analog to digital and visa-versa depend on the direction. A/D Converter also connects to the Encoder from where it receives information about when to trigger a pulse. The A/D converter is referred to as Electronic Unit(s).

### 3.1.3 Monitor/PC

The monitor or PC is used to visualize the GPR information in real time and to operate the system. Depending on the type of monitor, or if a PC is used, GPR data can be stored for later processing.

### **3.1.4 Control unit**

The Control unit is the brain center of the GPR system and is responsible for coordinating the operation of the subordinate components.

### **3.1.5 Antennas**

While the Control Unit is performing the functions of the brain and Antennas are the legs, doing the work of transmitting radar signals and receiving the reflected waves. As a general rule, the frequency of the antenna determines the depth of penetration and the resolution – the higher the frequency the better the resolution but at the expense of the depth of penetration.

## **3.2 Basic working principles**

The Encoder is the starting point for each measurement cycle. The A/D Converter connects to the Encoder from where it receives trigger requests to pulse a radar signal. On receipt of a trigger request, the A/D Converter passes the request to the Control Unit where a digital radar Trig signal is generated and passed back to the A/D Converter for analog conversion.

The analog radar signal is then relayed to the  $T_x$  (transmitter) antenna to pulse the target area and at the same time a signal is sent to inform the  $R_x$  (Receiver) antenna that a pulse has been sent and to expect reflected waves. Each radar pulse is digitally encoded so that matching of transmitted and reflected signals can be performed. Reflected waves from the  $T_x$  pulse are then captured by the  $R_x$  antenna and relayed to the A/D Converter for digitalizing. This digitized information is then passed to the Control Unit where it is interpreted and buffered for relay to the monitor and/or data storage device (usually a PC). This process is repeated as the GPR is moved across the surface of the target and at each measurement cycle, initiated by the Encoder, a GPR profile (often referred as radargram) of the subsurface is developed.

### 3.3 GPR antenna frequency description

Following the flowchart (Fig. 3.3) describes the antenna frequency description. For low frequency antennas, the wavelength will be longer and the size of the antenna is bigger. These antennas can be adopted for deeper ground penetration depths, however, with lower resolution and lower sensitivity. On the other hand, higher frequency antennas may be adopted for a shallow depth range with higher resolution and sensitivities. In this research study 1.6 GHz and 500 MHz antennas were used.

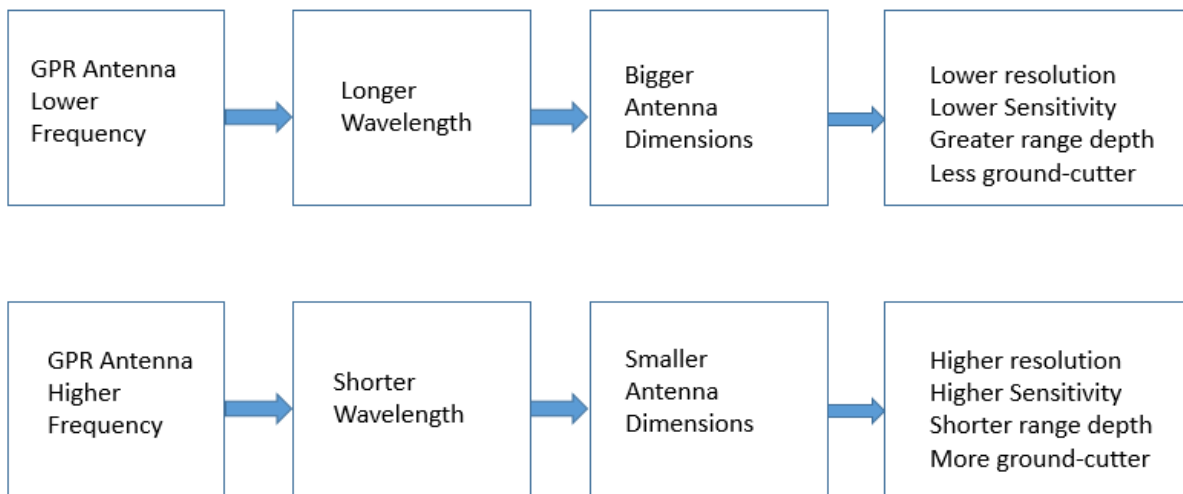


**Fig.3.3:** Flow-chart showing antenna frequency description

### 3.4 Test procedure

Prior to the start of GPR testing there are certain important settings that need to be taken care of for obtaining a good data. Firstly, the analysis has to be set to be 2D/3D as shown in Figure 3.4. A new project has to be selected and the settings are to be adjusted by selecting the settings symbol from the options available as shown in Figure 3.5. The slots to which the antenna has been connected has to be correctly set on the monitor and then the channel through which the data are obtained has to be set

correctly, i.e., Channel B1 for 1.6GHz antenna and Channel A for 500 MHz antenna and also velocity for a particular material and wheel type of particular antenna are to be set accordingly as shown in Figure 3.6. One of the important things to be taken care of is the radar wave velocity. Each material has a prescribed set of velocity range. Testing can be done by exactly knowing the material velocity from experimental study or randomly setting some three to four velocities given in the range or else it can be exactly obtained if there are any hyperbolic reflections observed in the radargram. If there are any hyperbolic reflections observed, the exact velocity, which is suitable for the test can be obtained in the post processing done in software irrespective of the velocity set during testing. As the project is started a signal dialog box appears at the right side of the monitor and the first peak of the signal from the antenna has to be set at zero level before the start by using a setting called “Adjust Signal Position” as shown in Figure 3.7. The sampling frequency should be kept approximately ten times the main frequencies of antennas. The colour palette of radargram and zero level can be adjusted from display parameter setting as shown in Figure 3.8. Once the testing is completed, the raw data has to be copied in a removable drive from the automatically saved files as shown in Figure 3.9. The radargram as obtained from GPR without any filters is shown in Figure 3.10. So the processing is done in a software called Reflex-W. In the software certain corrections/filters related to background removal, gain function, migration, running average is applied as shown in Figure 3.11. The background removal filter can eliminate temporally consistent noise from the whole profile and therefore makes signals visible, previously covered by this noise. The linear gain filter is applied in order to compensate for any damping or geometric spreading losses. The running average filter is applied to suppress trace dependent noise. The migration filter is used to contract strong diffractions to a minimum. Apart from these filters contrast of the image, hyperbola fitting, color palette of the radargram, velocity adjustment, depth and distance adjustments can also be done in the software.



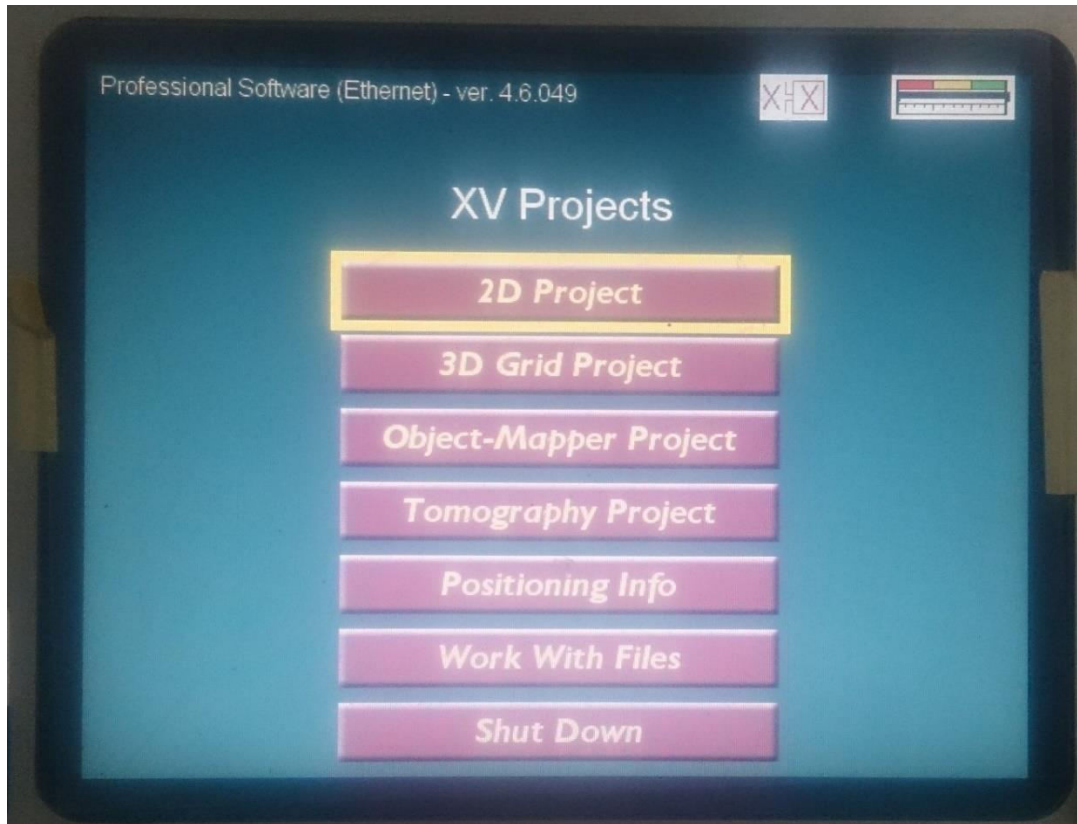


**Fig.3.4:** Various projects available for selection in GPR

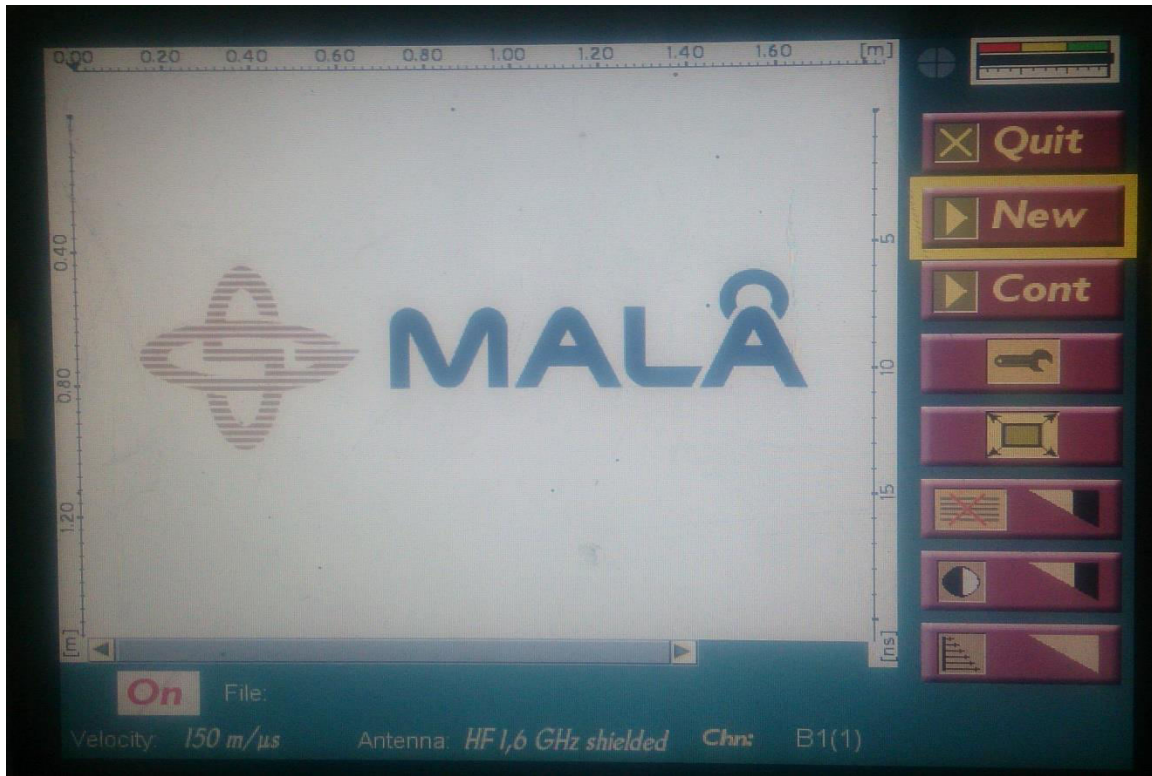


**Fig.3.5:** Different options available in 2D analysis

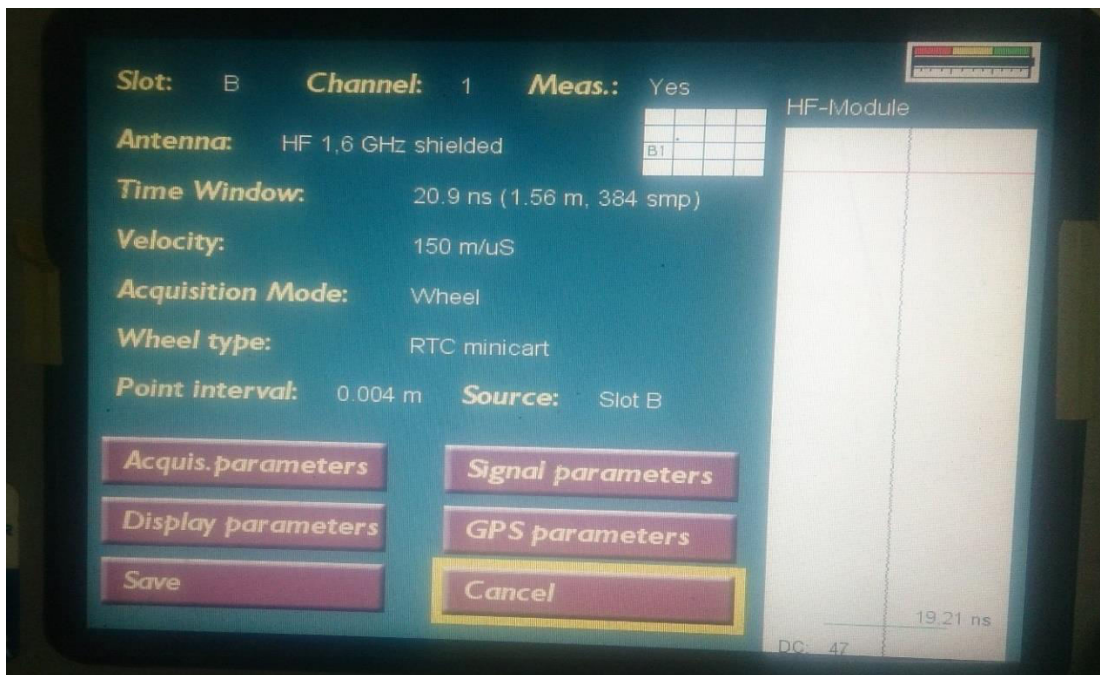


**Fig.3.6:** Preliminary settings for GPR survey

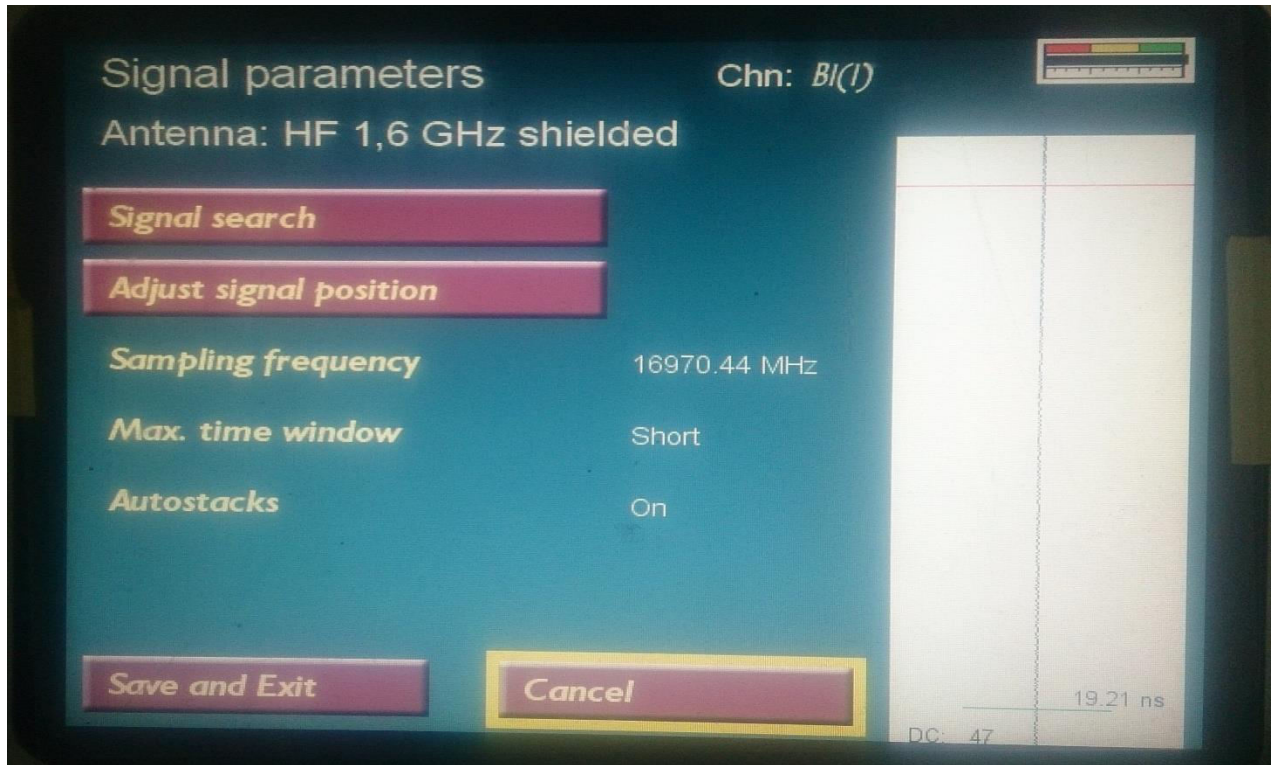


Fig.3.7: Signal parameter settings for GPR

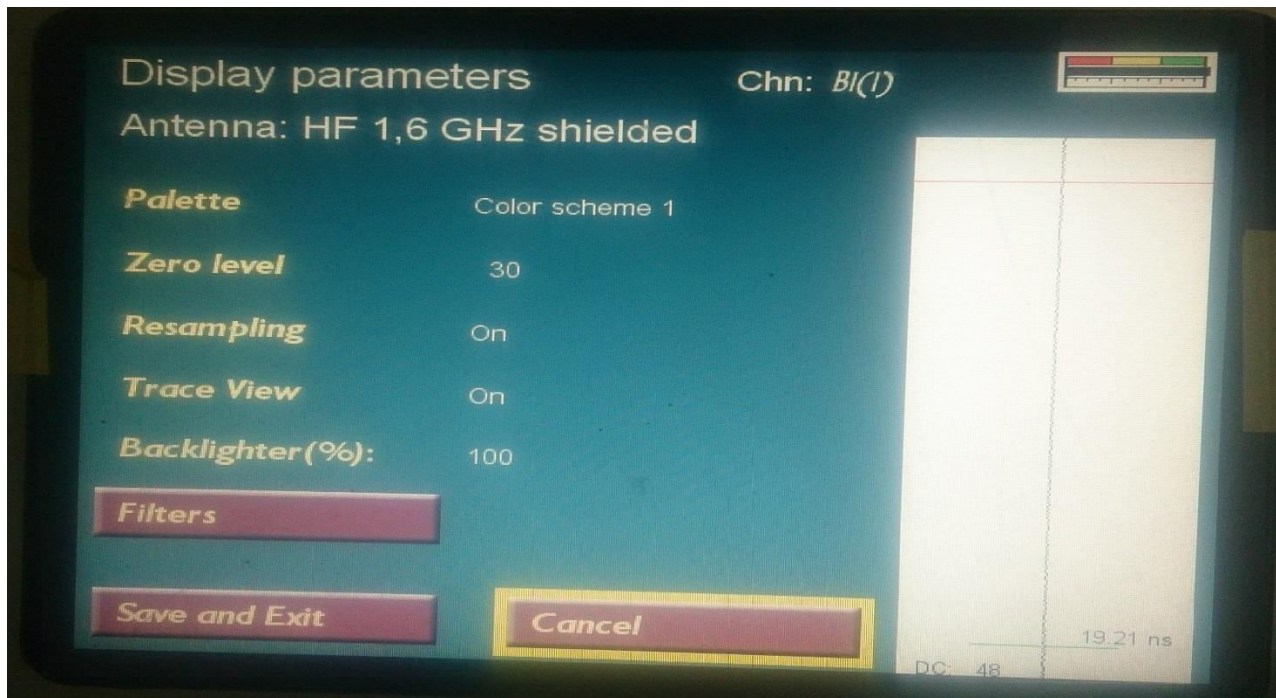
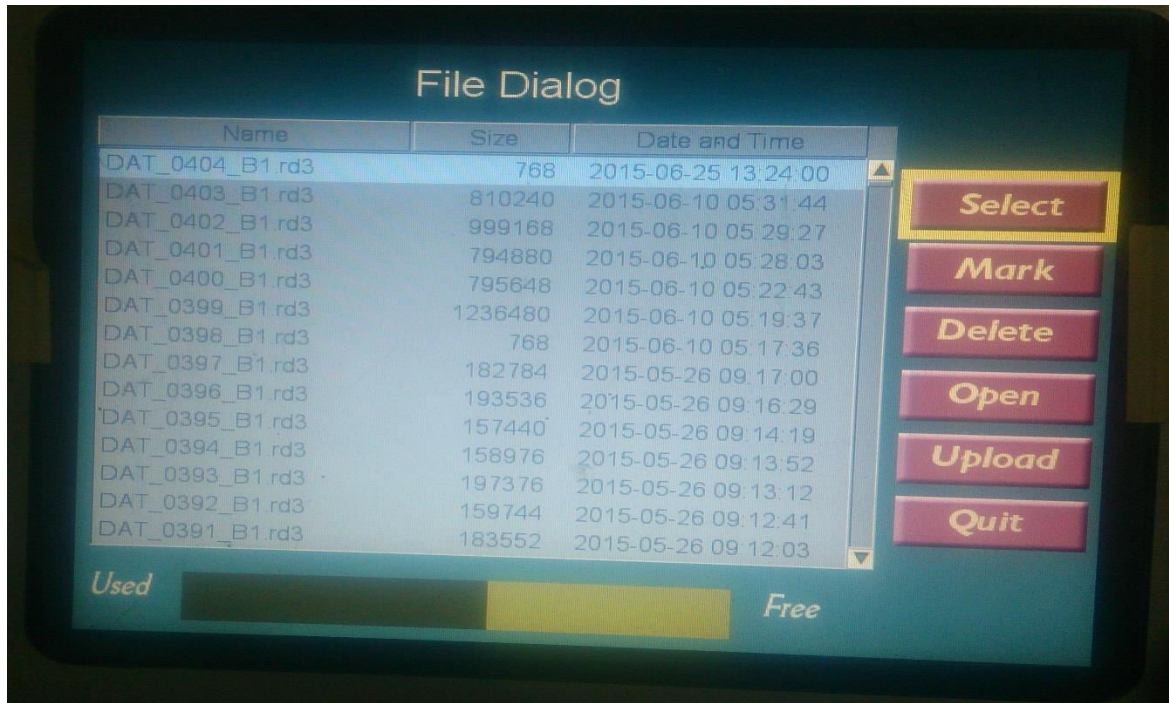
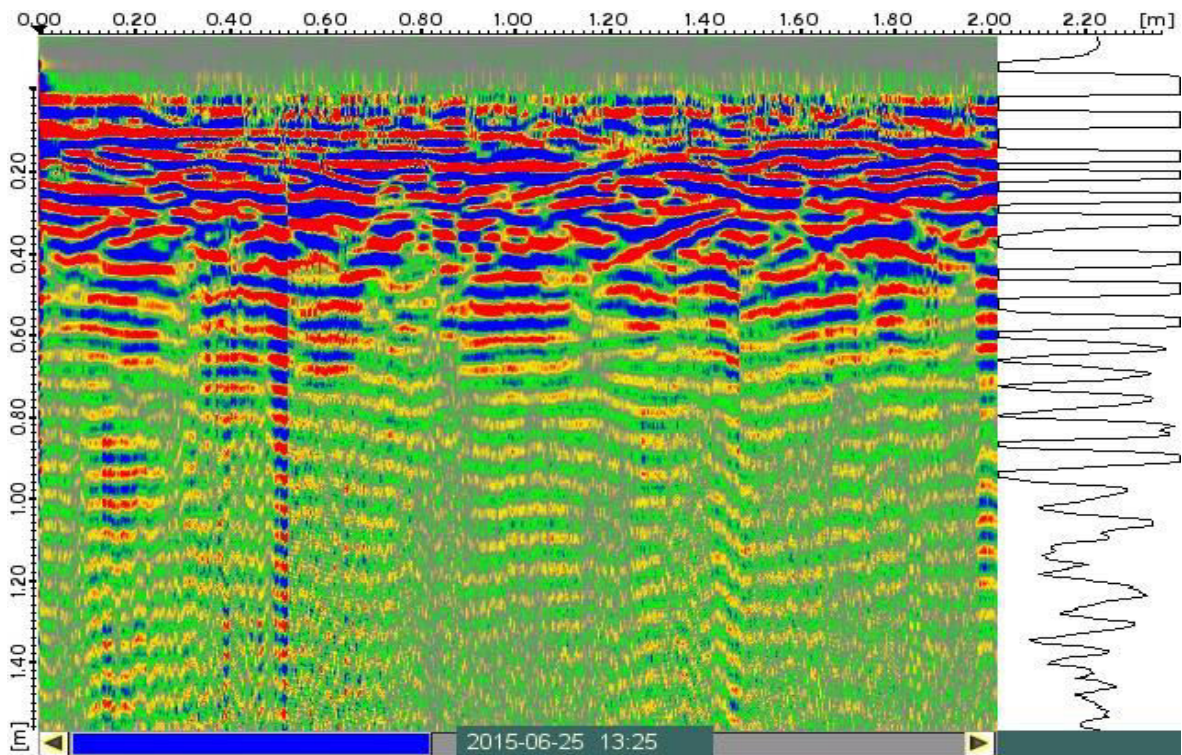


Fig.3.8: Display parameter settings for GPR



**Fig.3.9:** Saved files in the GPR



**Fig.3.10:** Radargram as obtained in the monitor

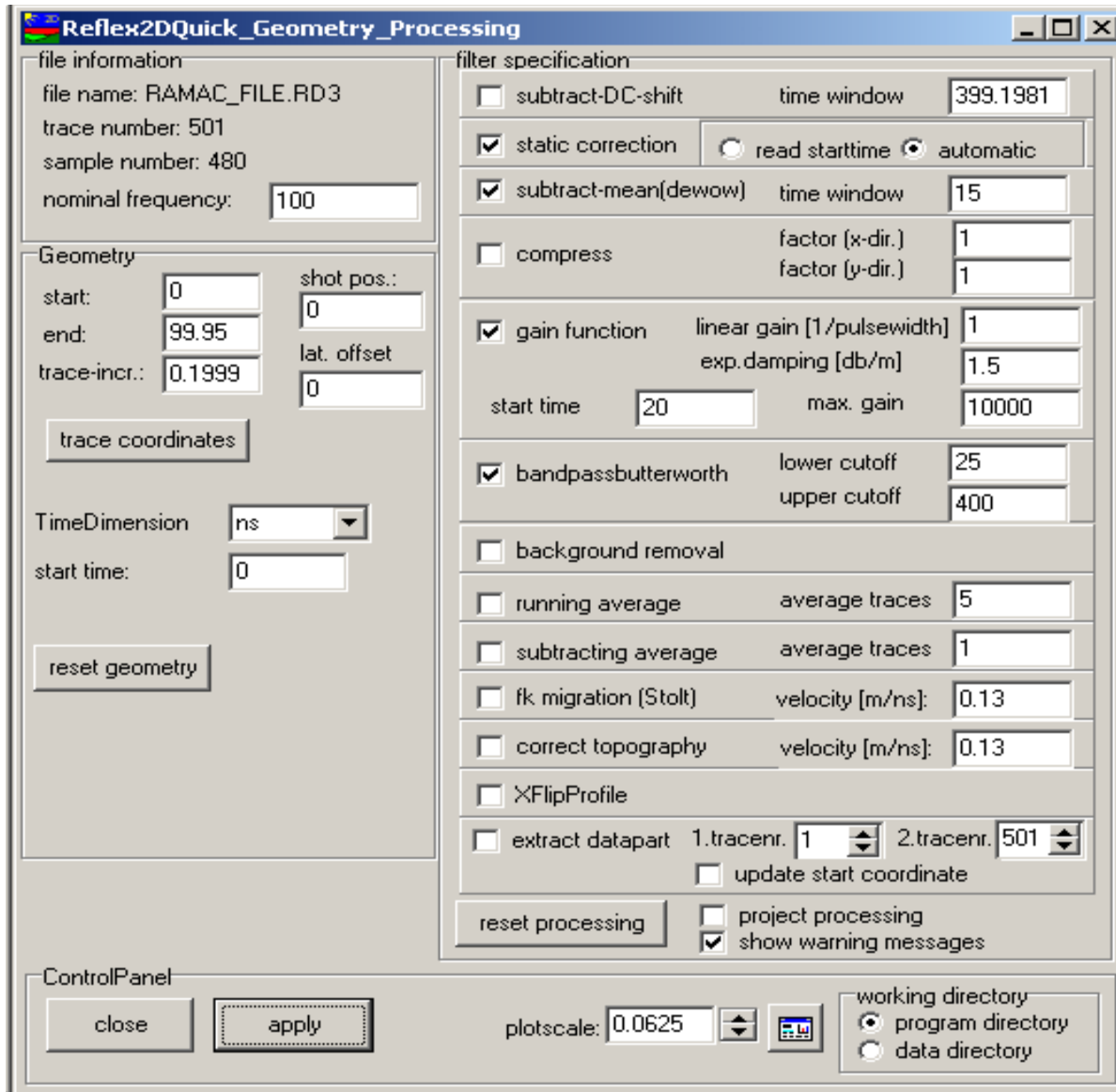


**Fig.3.11:** Filters and settings to be given in the software

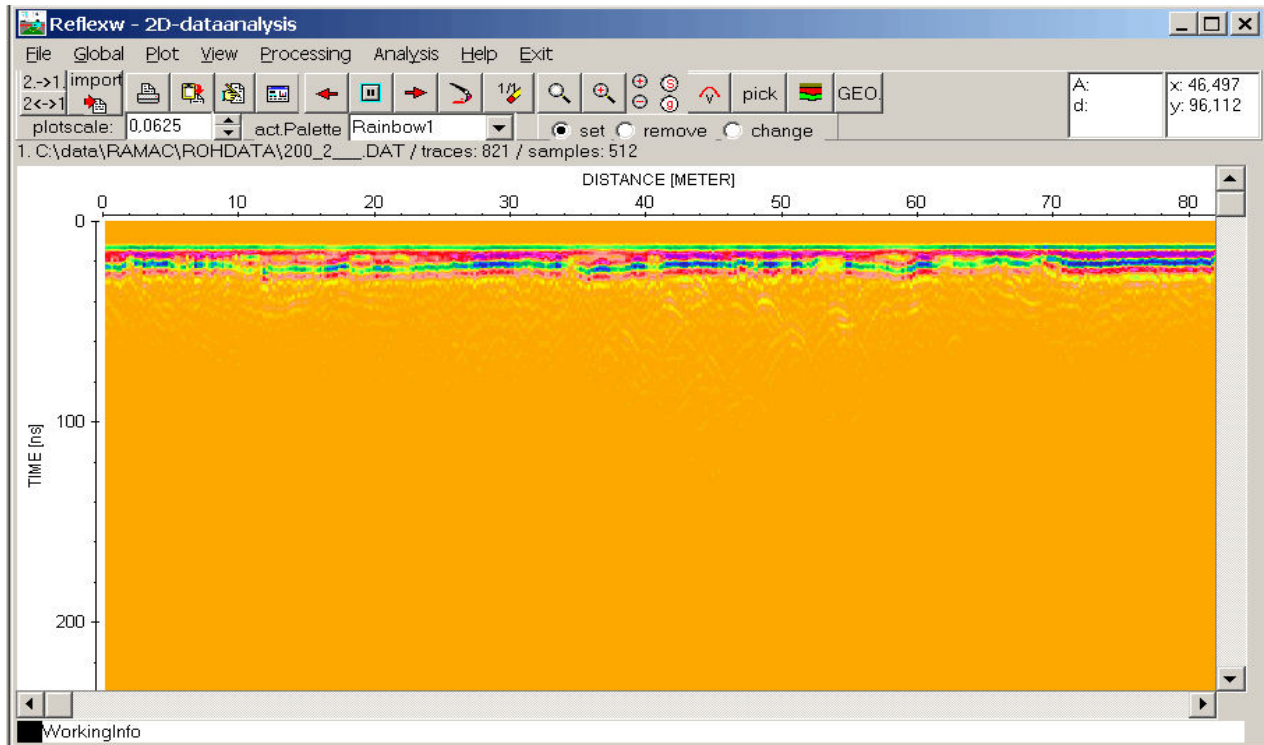


**Fig.3.12:** Profile shown in the software after processing

### 3.5 Calibration

Before adopting the GPR technic on real time pavement testing, several calibration studies have been performed as follows:

- Case 1: Identification of re-bars in an RC Concrete Slab
- Case 2: Identification of buried objects in a calibration test-pit (Clay)
- Case 3: Identification of buried objects and material changes in a calibration test-pit (Sand)

#### 3.5.1 Case 1:

In the first case GPR surveys were performed on a concrete slab in order to identify the reinforcement details such as reinforcement of re-bars, thickness of slab, number of bars in the test area, spacing between the bars.

Since the thickness of the slab will be less than 0.3m, 1.6GHz antenna has been used, as shown in Figure 3.13, as it gives a good resolution at such a depth. Two dimensional analysis was done in a span of 2m. The raw radargram was processed in the Reflex-W software and the results were analyzed. To process the

radargram filters such as background filter, zero level correction, velocity adjustment, and linear gain is applied and the contrast is to be correctly adjusted. The resultant radargram is shown in Figure 3.14 with the projected hyperbola curves since the rebar's gives out hyperbolic reflections. As can be seen from the radargram the test span was 2m. Each hyperbolic reflection represents a rebar located in that area. Hyperbola fitting has been done in order to know the exact velocity. The slab thickness and the depth at which the reinforcement is placed can be determined from the radargram which are 180mm and 130mm respectively. Therefore the effective cover of the slab is 50mm. The number of rebars in the test area is ten which is equal to the number of hyperbolic reflections. The diameter can also be determined by a method called the hyperbola fitting technique as shown in Figure 3.15 which requires plotting of a generalized hyperbola with its coordinates in a graph paper and finding the asymptotes (*a* and *b*).

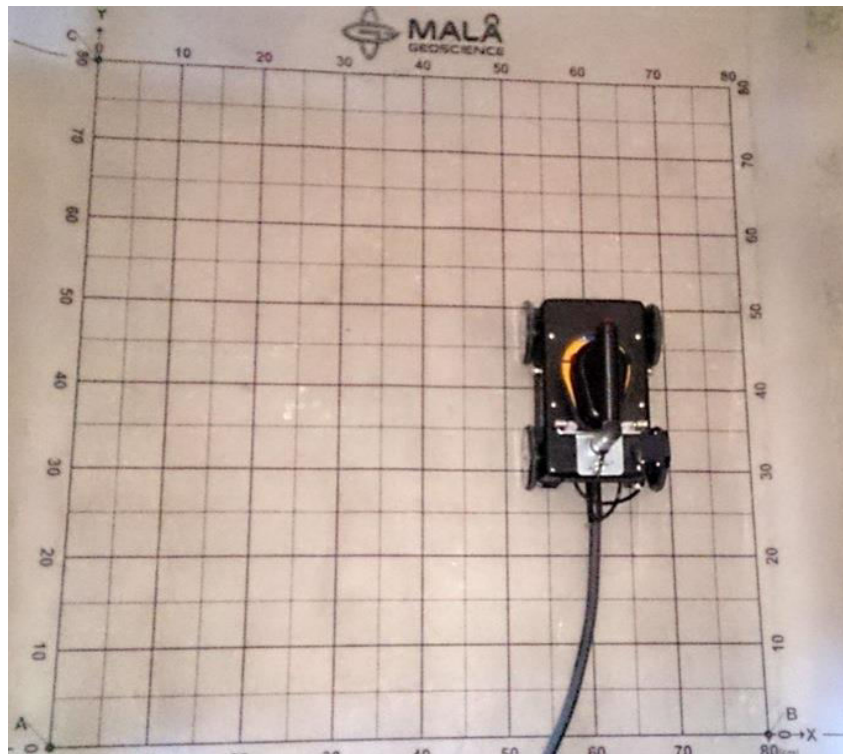


**Fig.3.13:** 1.6GHz antenna used for the test

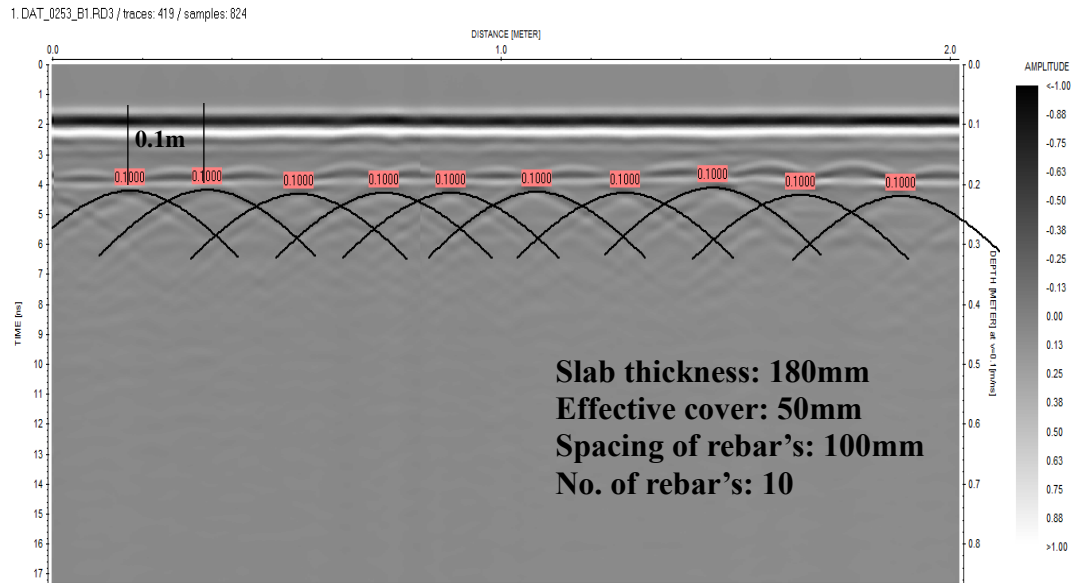


**Fig.3.14:** Processed Radargram with hyperbola fitting.

### 3.5.2 Calculation of Rebar diameter

The asymptotes  $a$  and  $b$  can be calculated as follows:



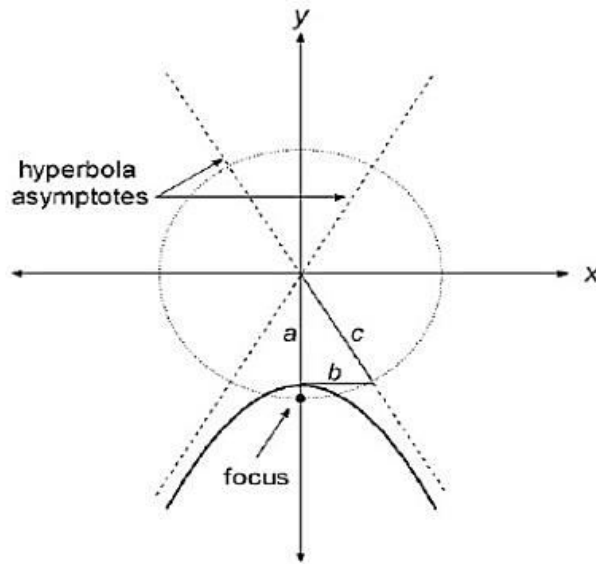


**Fig.3.15:** General Hyperbola with its asymptotes

$$a = t_0 + \frac{2R}{v} \dots\dots\dots(1)$$

$$b = \frac{v}{2} \left( t_0 + \frac{2R}{v} \right) \dots\dots\dots(2)$$

From the obtained radargram one single hyperbola along with its coordinates is selected and plotted manually in a graph paper to obtain the values of a and b. The values from the radargram (Fig. 3.14) are:

a=2.31

b=0.115

v=0.1 m/ns

t=3.9 ns

The diameters from equations 1 and 2 obtained are 11 mm and 10 mm respectively. Generally, the rebar diameter is either 10mm or 12mm. Therefore the actual diameter of the rebar may be determined based on whether the rebar is a main reinforcement or secondary. This can be evaluated based on the overall dimensions of the slab (one way or two way slab).

### 3.5.3 Case 2:

In the second case the GPR is calibrated on a test pit excavated near the tennis court in IIT Hyderabad campus, ODF. The test pit is of 10 m length, 1.5 m wide and 0.5m depth as shown in Figure 3.16. The objects of known dimensions are placed at pre-defined locations as shown in the Figures 3.16 and 3.17 to identify through the GPR testing. The antenna used in this testing is 500 MHz frequency since the depth of interest is 0.5 m. After all the objects are placed at the predefined locations, the compaction of test-pit was carried out. Figure 3.18 shows the compacted test pit with buried objects. The white color markings show the traversing locations of the GPR surveys.

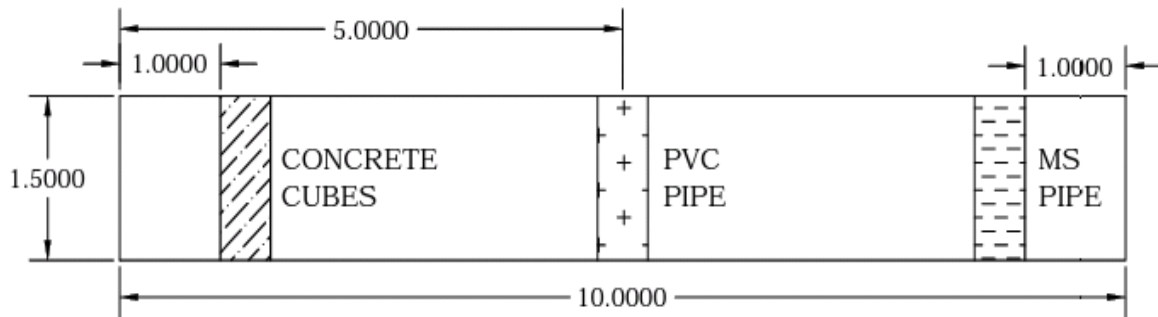


Fig. 3.16a: Plan view of the test pit

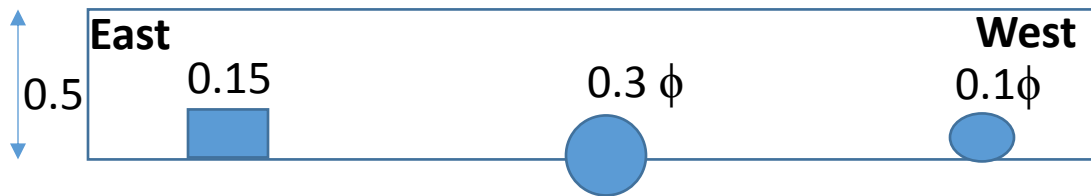
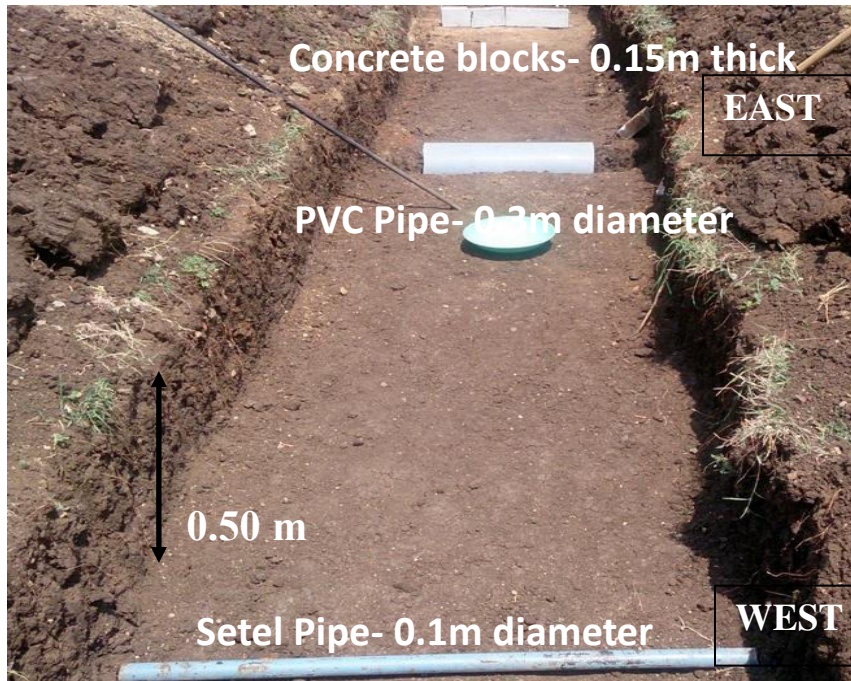
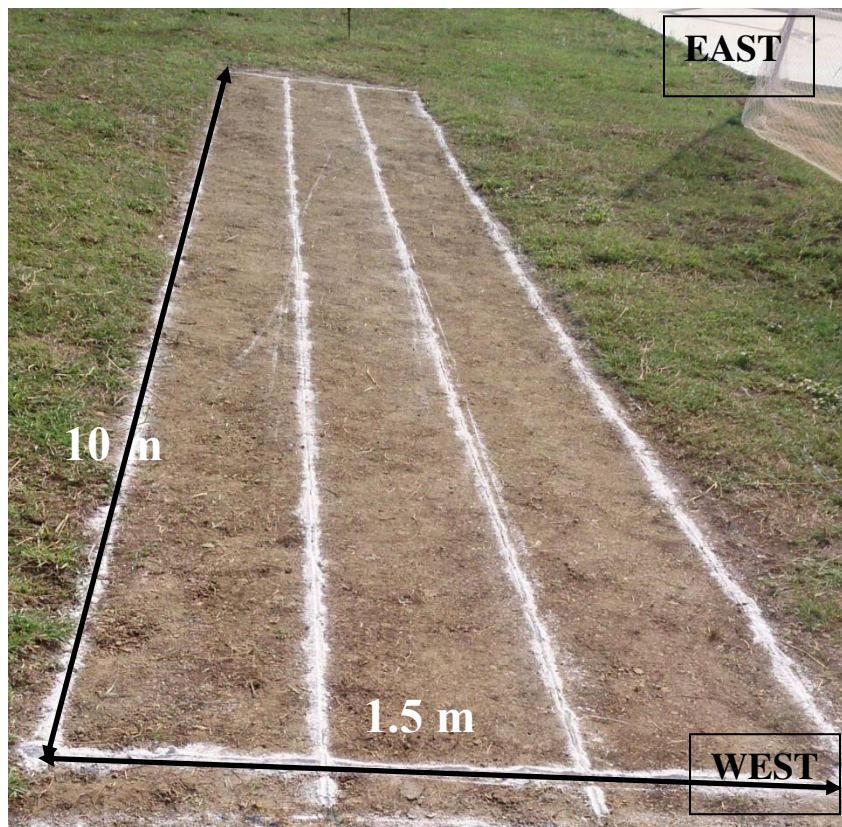


Fig. 3.16b: Cross section of the test pit

**Fig.3.16:** Plan & c/s of the calibration test pit (all dimensions are in meters)



**Fig.3.17:** Test pit with buried objects



**Fig.3.18:** Test-pit after compaction

The compaction of test pit was done using a roller of 100 kg in 3 layers at its maximum dry density and optimum moisture content. Later, the GPR survey has been performed 2m ahead of the length of the compacted test pit to see the changes between the natural ground surface (GS) and the compacted GS using the GPR traversing from West to East direction and the data has been processed in the software and the radargrams are analyzed. Figure 3.19 shows the raw/unprocessed radargram before applying the filters and required adjustments.

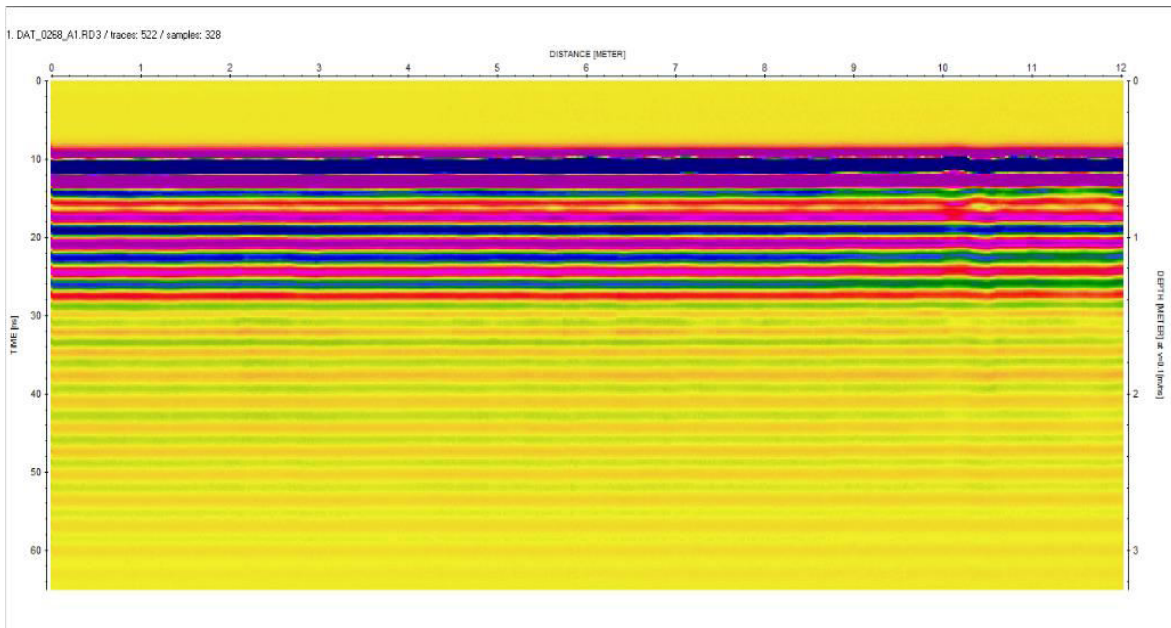


**Fig.3.19:** Unprocessed Radargram

Figure 3.20 shows the processed radargram after application of all the filters. Figure 3.20 depicts that the compacted GS was showing lighter intensity which means that the density of that layer is lower than the natural GS. This is because, the compacted layer is weaker than the naturally compacted ground surface. There are hyperbolic reflections at the location of PVC pipe and the hyperbolic fitting has been done and the diameter of the pipe is determined. Other buried objects such as steel pipe of small diameter, concrete blocks etc. could not be detected due to moist nature of the compacted clay. There is a noise/disturbance noted at these locations and hence the location of these objects are positioned, however, it is difficult to determine the size of each object. The survey would have given much more information if the compaction in the test pit is higher than the natural soil.

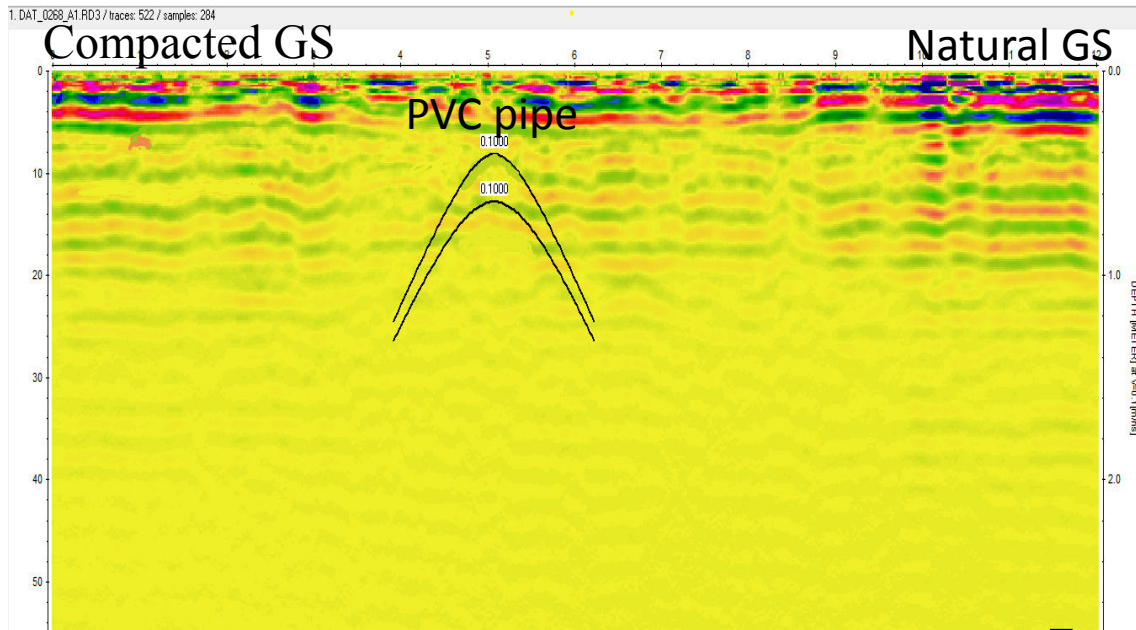


**Fig.3.20:** Processed Radargram

The diameter of PVC pipe can be determined as follows:

$$d = \frac{v \times t}{2} = \frac{0.1 \times 6}{2} = 0.3m$$

The original dimension of the pipe is matching with the obtained one. Also the depth at which the bottom of the pipe is located can be obtained from the radargram i.e.at 0.6m. Hence it can be said that the PVC material can be easily detected with higher accuracy with GPR.

### 3.5.4 Case 3:

In this case a test-pit of 0.9m ×0.9m×0.3m was constructed using concrete cubes and beams. The cross section and plan view of the test pit with the buried objects are shown in the Figure 3.21. Exactly at the center of test-pit a PVC pipe of 0.3m diameter was placed. A metal pipe of 0.1m at a distance of 0.17m from the west direction to the pit was placed and a small circular steel pipe of diameter 0.045m at a distance of 0.82m from west direction were placed as shown in Figure 3.22. An already calibrated sand has been used in this test. The calibration of the sand used in this study is shown in Figure 3.23. The sand has been pluviated into the pit using the raining technique as shown in Figure 3.24.

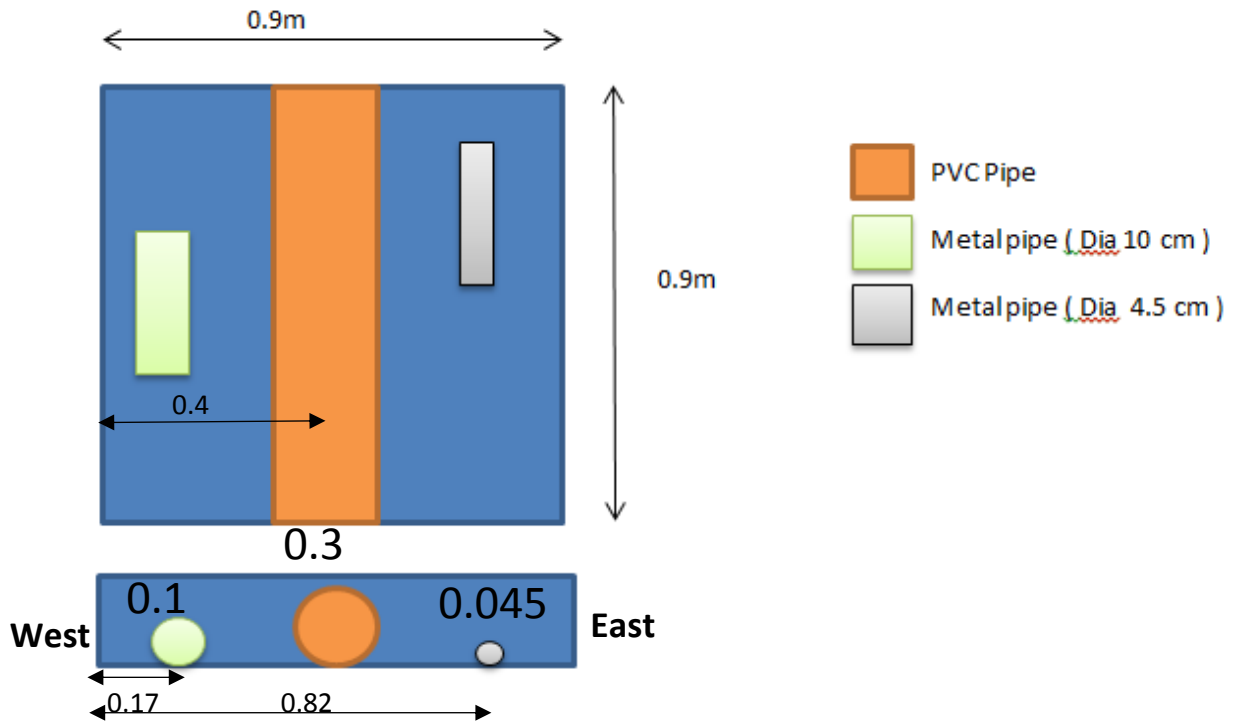


**Fig.3.21:** Plan and Elevation of test-pit (All dimensions in 'm')



**Fig.3.22:** Test-pit with different objects placed

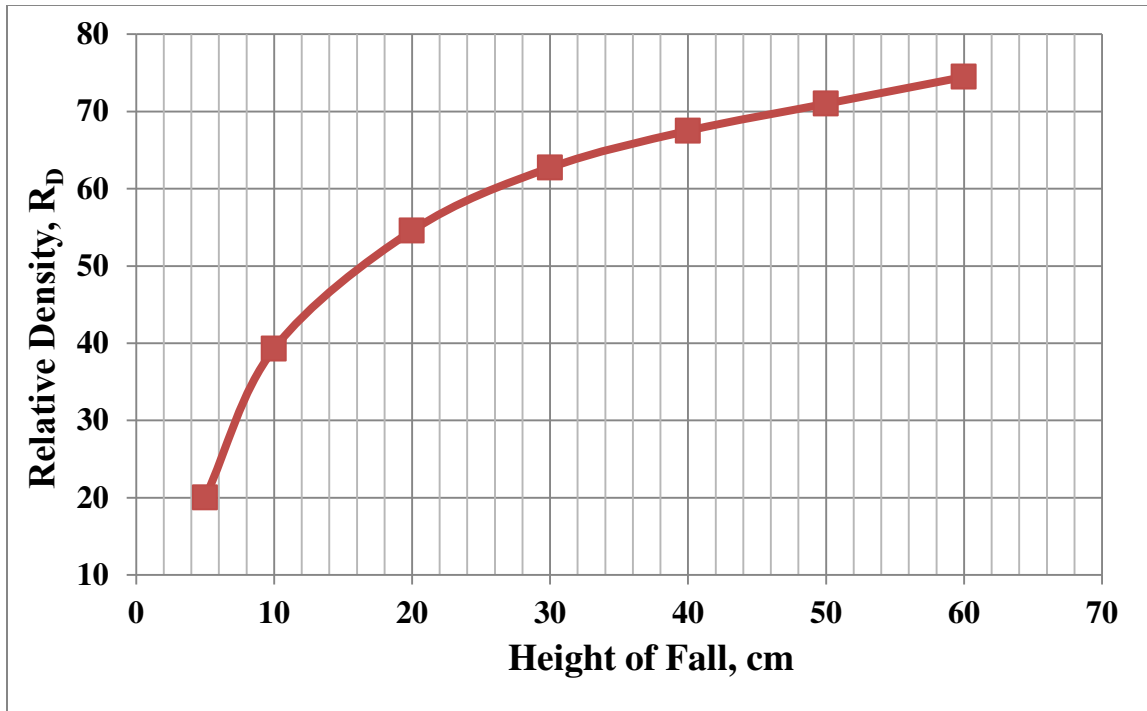


**Fig.3.23:** Relative density calibration chart of sand



**Fig.3.24:** Filling of sand using pluviation technique

After filling the test pit, a grid sheet has been placed on the test pit and two GPR surveys have been performed along the directions pointed in the Figure 3.25. Testing has been done using 1.6GHz antenna since the depth of interest was 0.3m from west to east direction. The velocity of radar-wave was set to 0.15m/ns. The data was processed using the Reflex-W software and the respective radargrams are shown in Figures 3.26 and 3.27. Since the first survey was done at the edge of the test pit only reflections due to PVC pipe are identified as shown in Figure 3.26. Hyperbola has been fit to the obtained hyperbolic pattern and the diameter of PVC pipe has been determined. It was also observed that the bottom of the PVC pipe is located at 0.3m from the surface, which confirms the depth of the test pit.

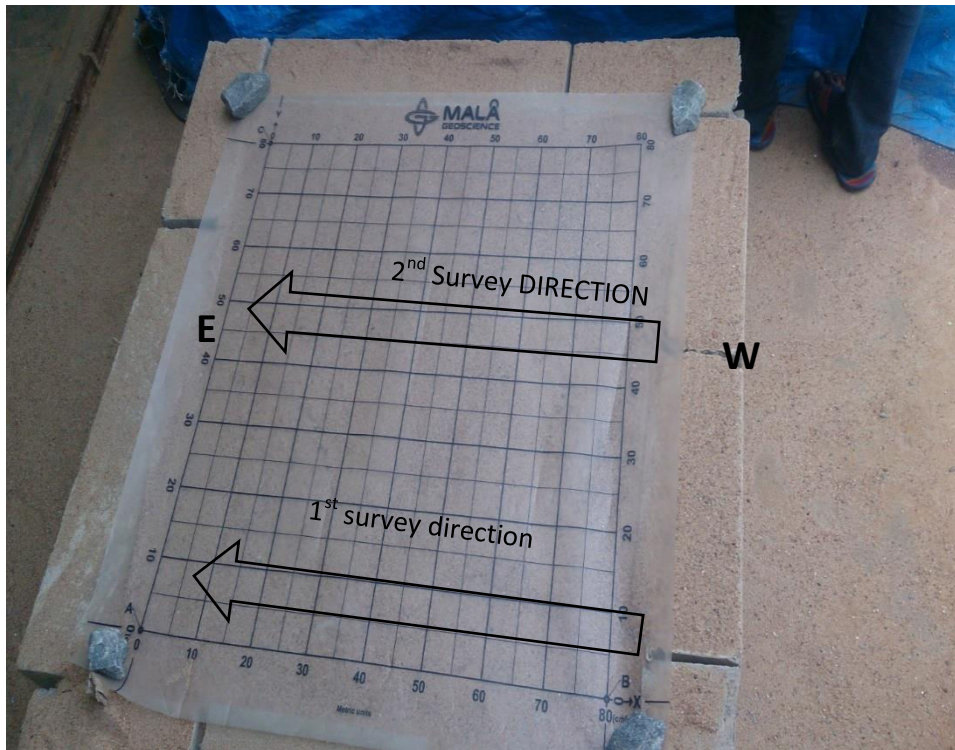


**Fig.3.25:** Test-pit after completely filled with sand



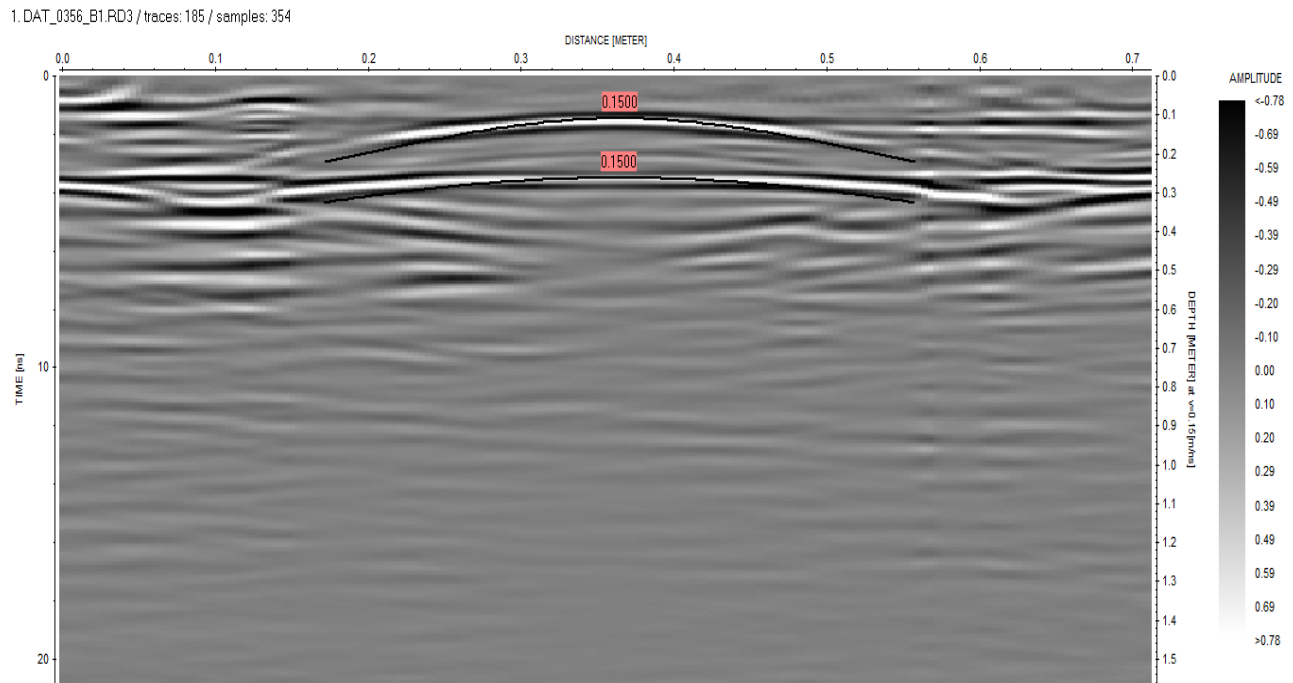


**Fig.3.26:** Processed radargram showing PVC pipe

### PVC Pipe Diameter

The diameter of the PVC pipe is determined with the following relation:

$$d = \frac{v \times t}{2} = \frac{0.15 \times 4}{2} = 0.3m$$

The original dimension of PVC pipe is matching to that of calculated one.

The second survey was done at the center of the test-pit. There were two hyperbolic reflections identified in the radargram, one is of PVC pipe and the other is of steel pipe at the right extreme disturbance due to smaller steel pipes has been observed as shown in Figure 3.27. Hyperbolic fitting method was adopted to trace the steel pipe and the diameter was determined.

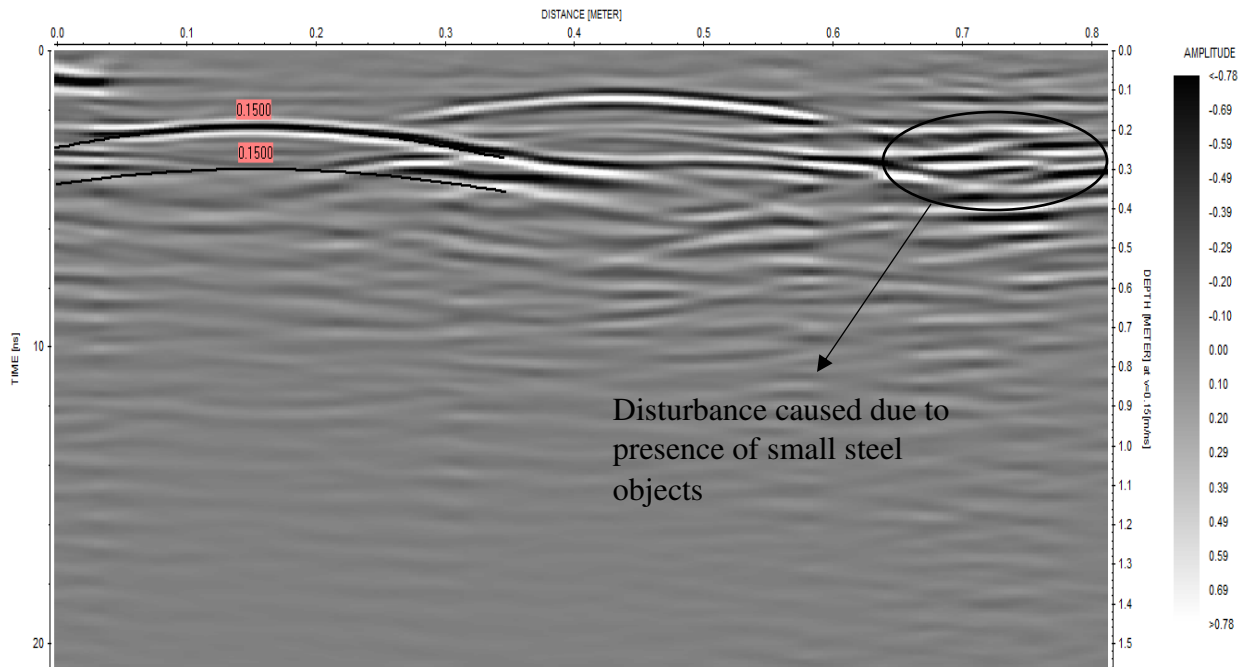


**Fig.3.27:** Processed radargram at the center of test-pit

### Steel Pipe Diameter

$$d = \frac{v \times t}{2} = \frac{0.15 \times 1.5}{2} = 0.105m$$

The calculated diameter of the Steel pipe was 0.105m which is almost equal to that of the original one of 0.1m.

### Calibration of GPR on Sand with Varying Relative Densities (Trail 1):

A test-pit of dimensions similar to the previous test was prepared near workshops of IITH. The test-pit was divided into two halves by placing concrete blocks exactly at the center along the length. In one half of the test-pit, on the east direction, a cylindrical concrete block of diameter 0.15m was placed and on the other half of the pit, on the west direction, a nearly round shaped stone of maximum width 0.17m was placed. The plan and cross-section of the test pit with the buried objects are shown in Figure 3.28. In the direction where the stone was placed, sand was filled in two layers using raining technique as shown in Figures 3.29, 3.30 and 3.31. The bottom half was filled with  $R_D$  75% and the top half was filled with  $R_D$  30% of the sand. The height of fall was obtained from the previously shown calibration graph (Fig. 3.23)

of the sand and it was 60cm for  $R_D = 75\%$  and 8cm for  $R_D = 30\%$ . The objective of this study is to identify the variation in radargram due to change in the density of the soil.

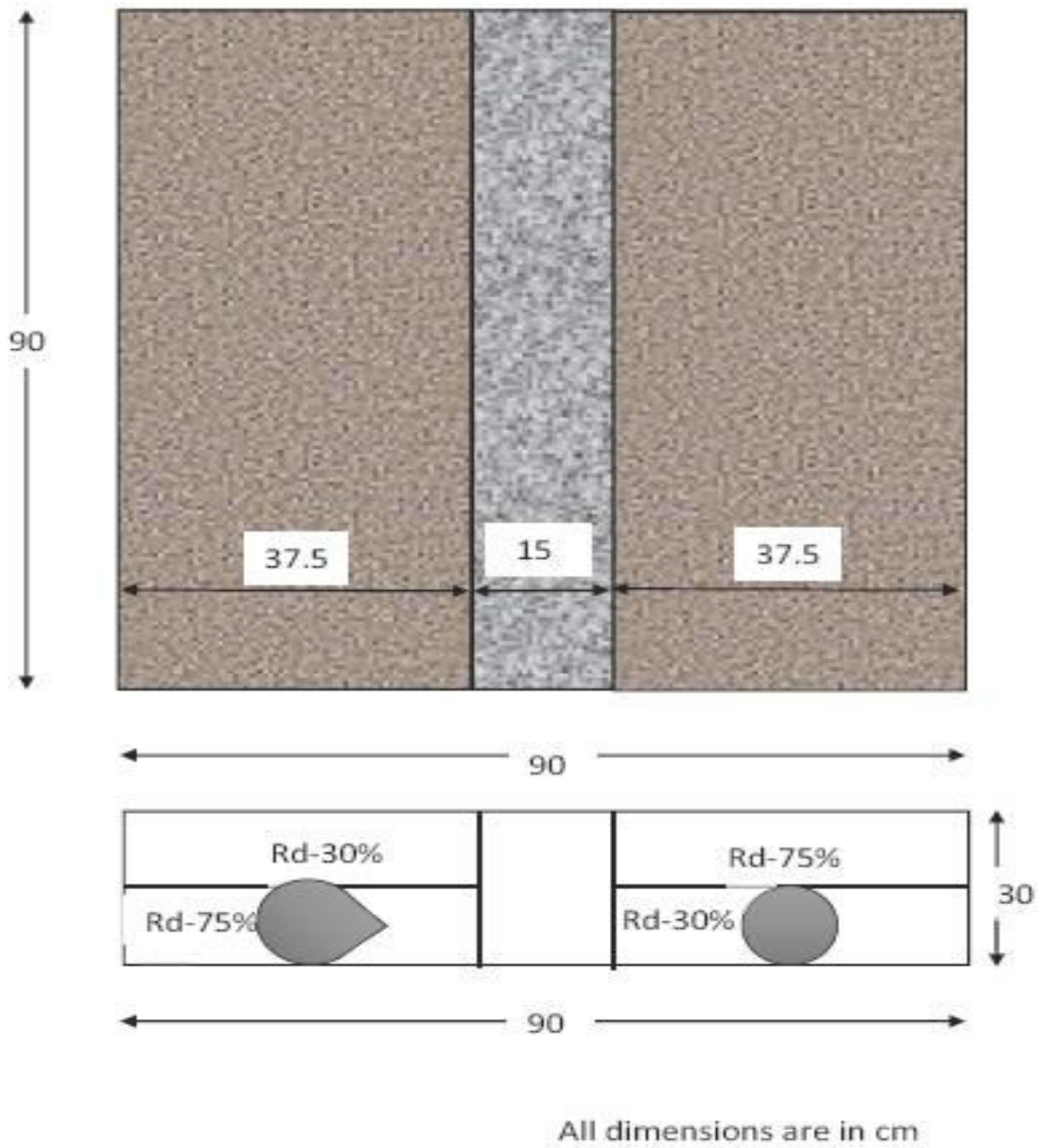


**Fig.3.28:** Plan and cross-section of test-pit



**Fig.3.29:** Test-pit showing sand being poured in the stone placed side

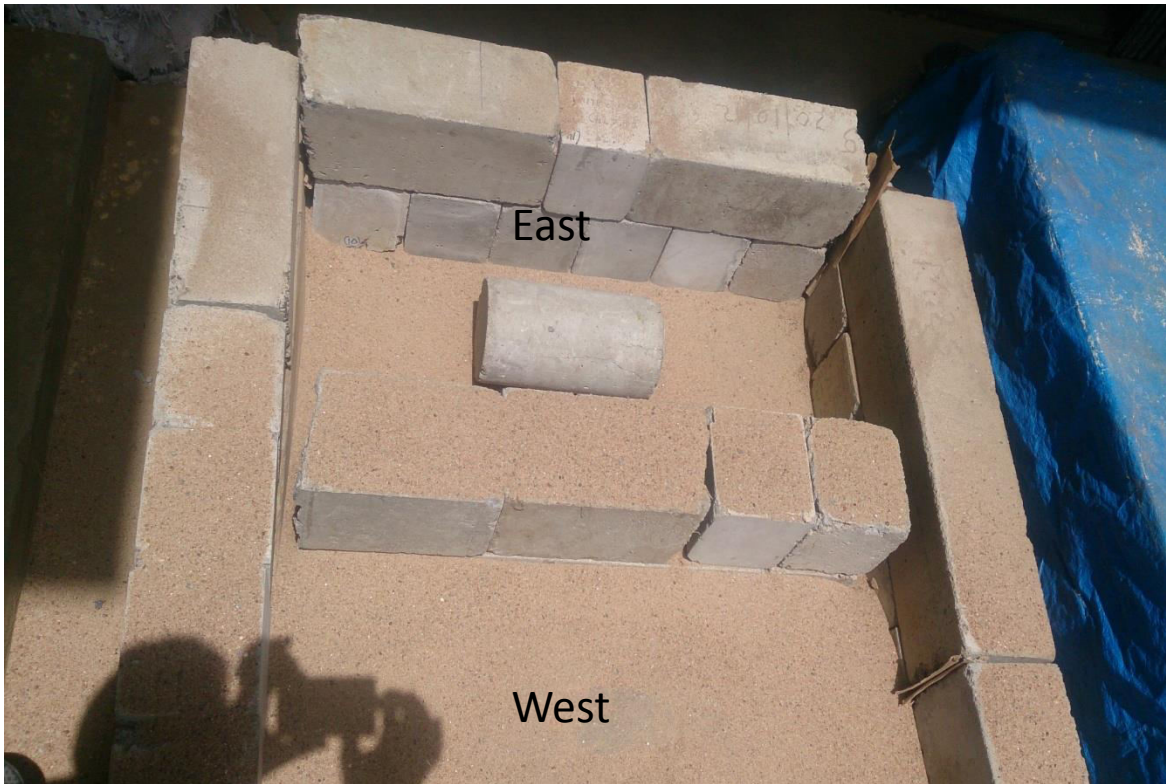


**Fig.3.30:** Test-pit showing the cylindrical concrete block placed



**Fig.3.31:** Test-pit after completely filling with sand

Testing was done from west to east direction of the pit using a 1.6GHz antenna with the radar-wave velocity set to 0.15m/ns. The data was processed in the software and the radargram shown in Figure 3.32 was obtained. The radargram was analysed by the hyperbolic curve fitting method to determine the diameter of the objects. In the radargram, the area where concrete blocks were present at the center of the test pit, no deflections/deviation in the radargram were observed indicating that the object is very stiff like a concrete as shown in Figure 3.32. These deflections are more prominent when the density of the overlying layer is higher. The reflections are weaker if the upper layers are loosely packed as shown in the Figure 3.32. In other words, the objects buried in denser layers produce better reflections than buried in weaker layers.

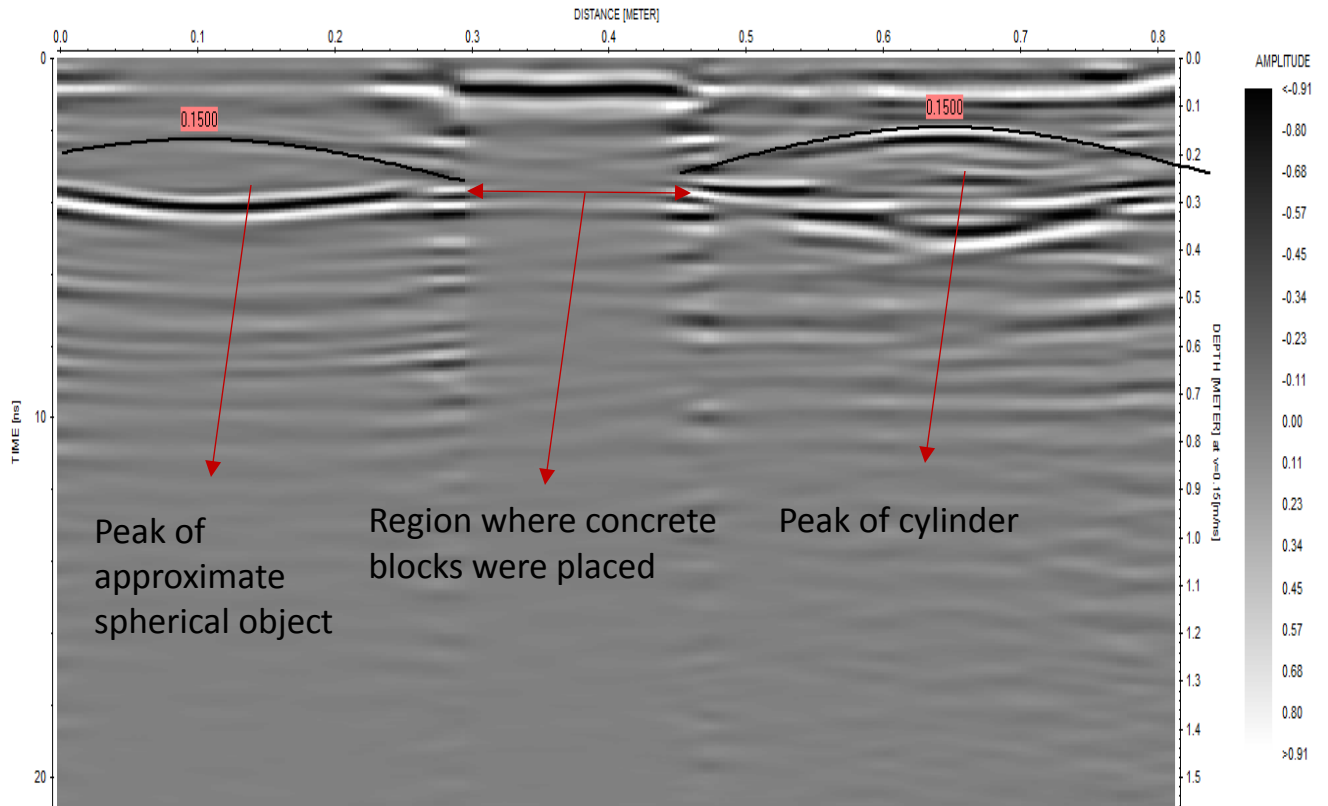


**Fig.3.32:** Processed radargram including hyperbola fitting

**Diameter of nearly round shaped stone:**

$$a = t_0 + \frac{2R}{v} \dots\dots\dots(1)$$

$$b = \frac{v}{2} \left( t_0 + \frac{2R}{v} \right) \dots\dots\dots(2)$$

From the obtained radargram one single hyperbola along with its coordinates is selected and plotted manually in a graph paper to obtain the values of asymptotes  $a$  and  $b$ . the values are:

$a=2.9$

$b=0.22$

$v=0.15$  m/ns

$t_0= 2$ ns

The diameters of the objects are obtained from the equations 1 and 2 are 13.5 cm and 14.1 cm respectively. The original dimension of the stone was 17cm. Hence the diameter was determined with a small percentage of error.

#### **Diameter of the cylinder:**

The same hyperbola fitting technique was used to determine the diameter of the cylindrical cube as well.

$$a=2.7$$

$$b=0.21$$

$$v=0.15 \text{ m/ns}$$

$$t_0= 1.9\text{ns}$$

The diameter of the from equation 1 and 2 obtained are 13cm and 14cm respectively. Original dimension of the cylindrical block was 15cm. Hence the diameter was determined with a small percentage of error.

#### **Calibration of GPR on Sand with Varying Relative Densities (Trial 2):**

A test pit of dimensions 0.8m×0.8m×0.3m has been prepared using concrete cubes and beams. The test pit is divided in to two halves by placing a row of concrete blocks the the centre of the pit. On one side of the pit, a cylindrical concrete block has been placed and on the other side a nearly round shaped stone has been placed. On the side where cylindrical concrete block was placed sand was filled by raining technique where, for the bottom half of the depth  $R_D$  75% was maintained and for the top half  $R_D$  30% was maintained. On the other side where a stone is placed  $R_D$  30% have been maintained in the bottom half and  $R_D$  75% for the top half. 1.6 GHz frequency antenna has been used for GPR analysis since the depth is 0.3m and also at such depths this antenna gives good data. A series of surveys were performed on this set-up and all the radargrams were analyzed. Figures 3.3 to 3.5 shows the test pit with buried objects and completely filled test pits.

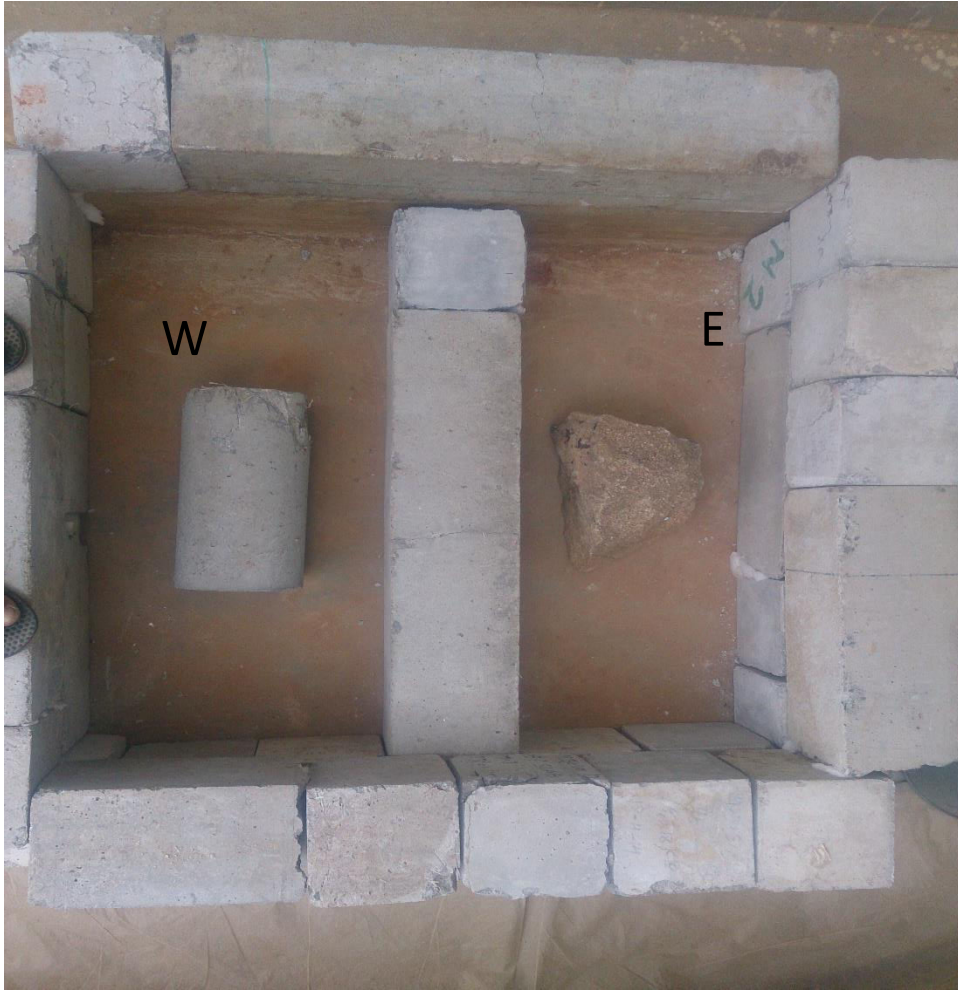


**Fig. 3.33:** Test set-up along with the objects placed



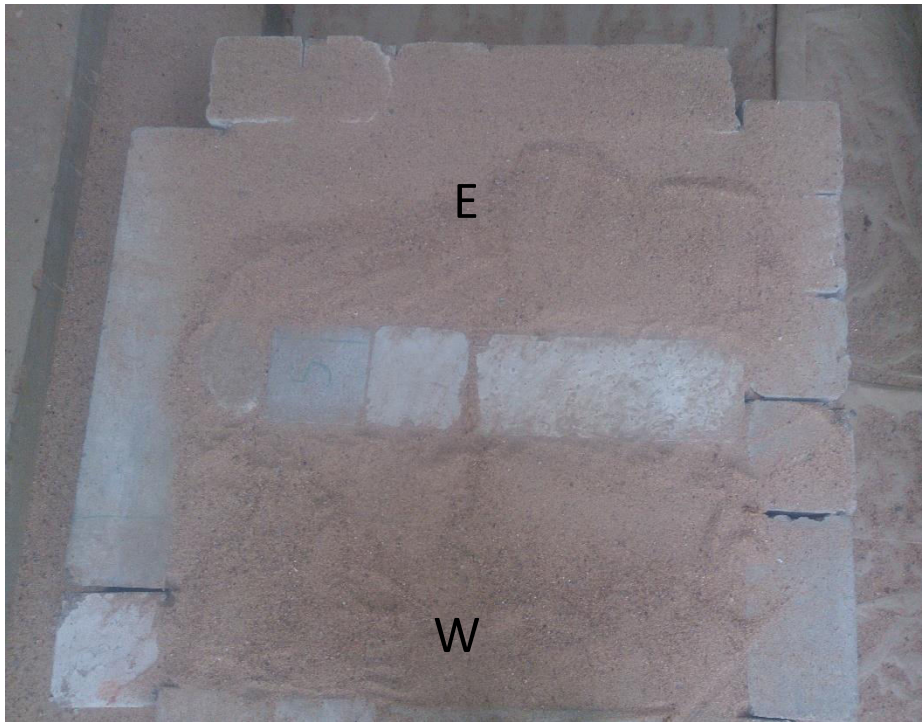


**Fig.3.34:** Test set-up after filling it with sand



**Fig.3.35:** Test set-up while running GPR

### Survey 1:

The first survey on the set-up has been run along the left edge of the test pit from west to east direction as shown in Figure 3.36, where the interference of the objects is not present. The objective of this survey is to see the variations in radargram in concrete and compacted sand layers. Figures 3.37 and 3.38 show the unprocessed and processed radargrams of the survey. The distance at which the concrete blocks were present (0.34m), the radargram is showing a sudden change in the reflection from that of the sand layer. and also under the blocks there were no layers as that of present in sand as shown in Figure 3.39. Also the distances were matching with that of the original plan. A vague distinction between the dense and loosely compacted layers can be noticed in this radar gram, however, the reflections are not remarkably different as there were no objects directly present underneath the line of survey.

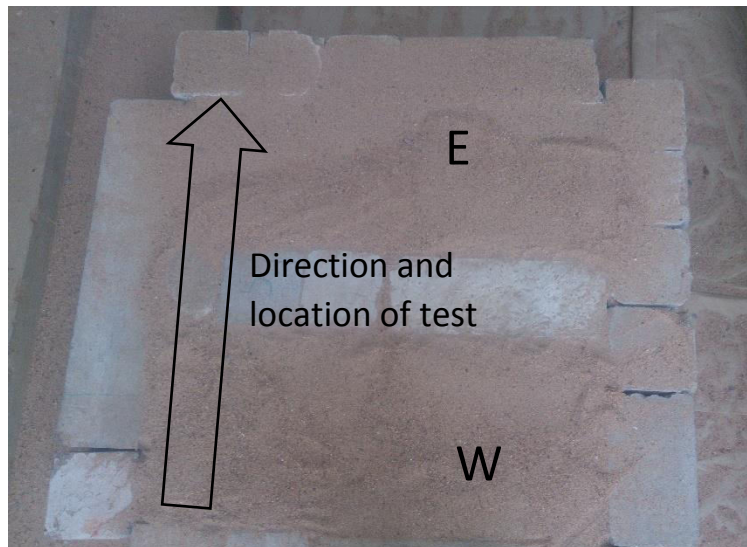


**Fig.3.36:** Test-pit shown along the direction and location of testing

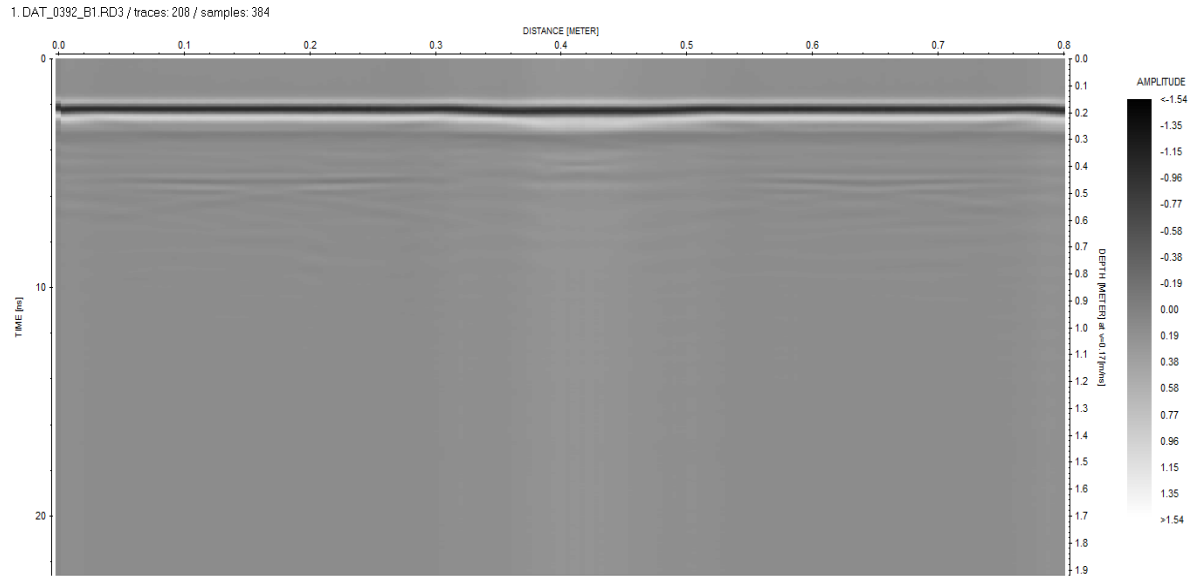


**Fig.3.37:** Unprocessed radargram

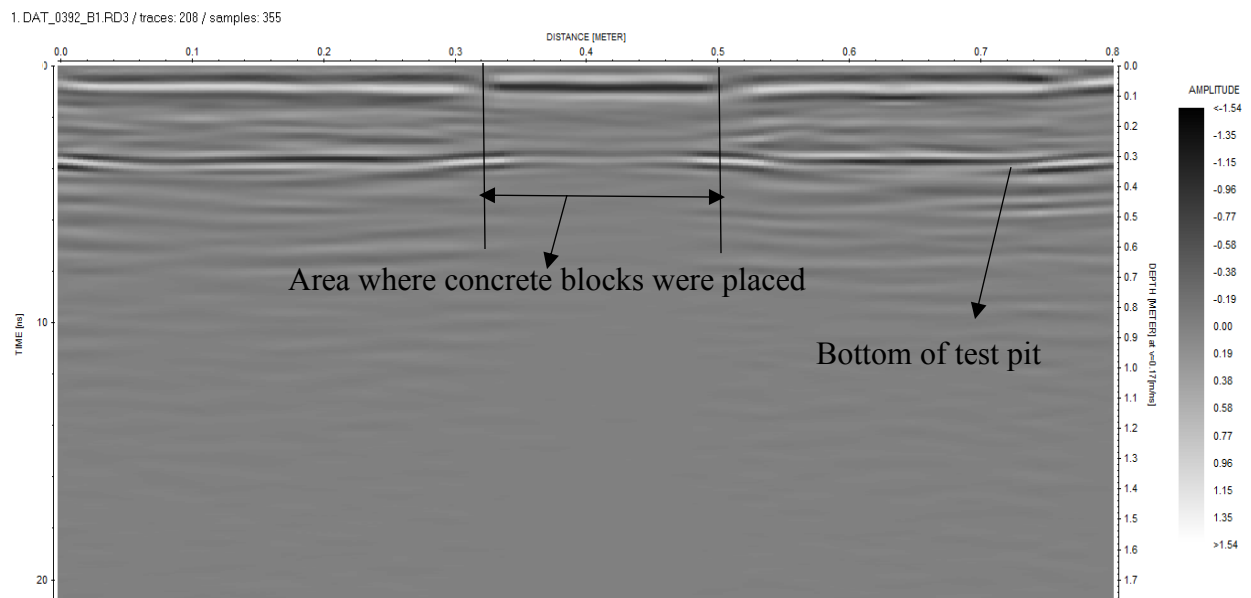


**Fig.3.38:** Processed radargram

## Survey 2:

Survey 2 has been done along the center line of the test-pit. The buried objects have been detected and also their dimensions were determined using a hyperbola fitting technique. Also, it has been observed that

the object which is placed in the density higher at the top and lower at the bottom showed good reflections.

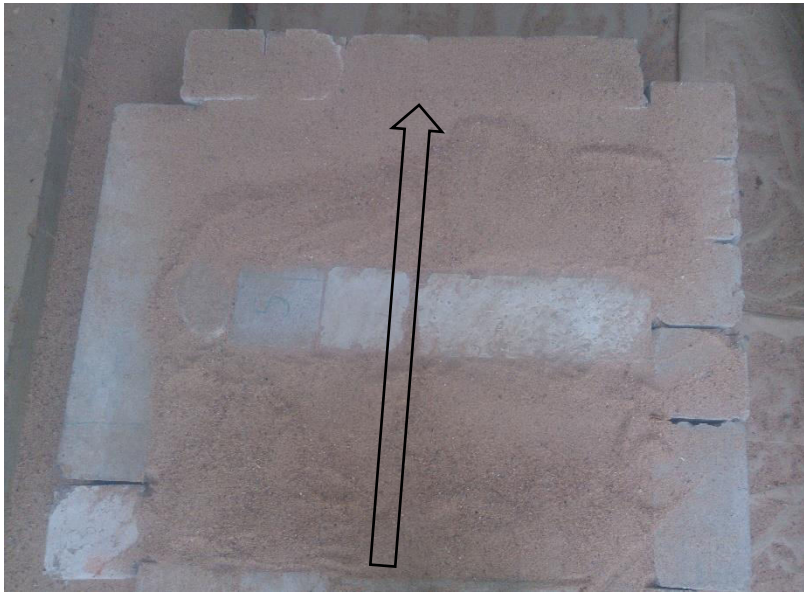


**Fig.3.39:** Test-pit with direction and location of test

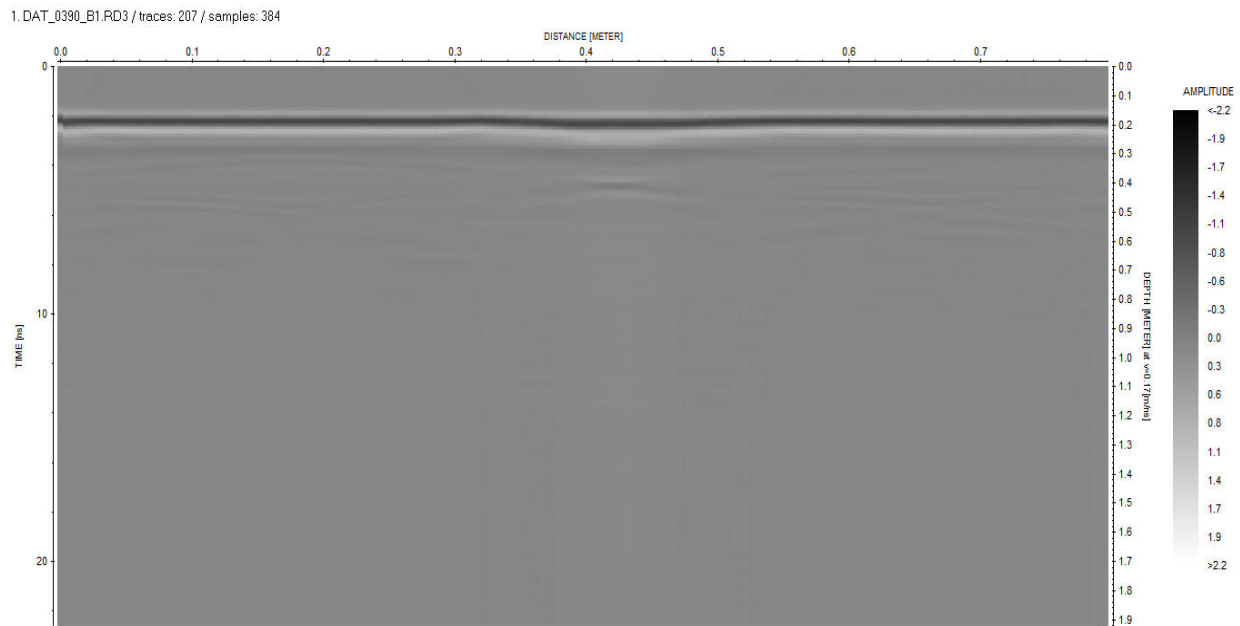


**Fig.3.40:** Unprocessed radargram

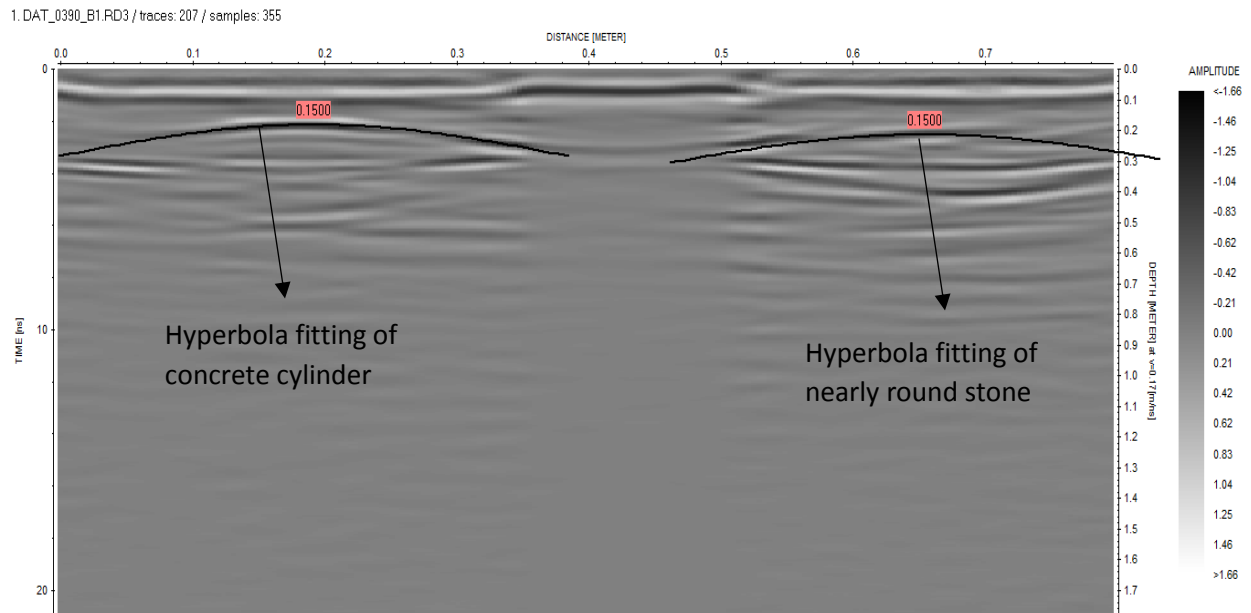


**Fig.3.41:** Processed radargram with hyperbola fitting

**Diameter of cylindrical concrete block:**

The same hyperbola fitting technique as mentioned previously was used to determine the diameter of the cylindrical concrete block.

$$a = t_0 + \frac{2R}{v} \dots\dots\dots(1)$$

$$b = \frac{v}{2} \left( t_0 + \frac{2R}{v} \right) \dots\dots\dots(2)$$

a=2.9

b=0.23

v=0.15 m/ns

t<sub>0</sub>= 2ns

The diameters from equation 1 and 2 obtained are 13.5cm and 14.1cm respectively. Original dimension of the cube was 15cm.

### **Diameter of nearly round shaped stone:**

Using the hyperbolic curve fitting method, the diameter of the spherical shaped stone can be obtained.

$$a=2.97$$

$$b=0.23$$

$$v=0.15 \text{ m/ns}$$

$$t_0= 2.1\text{ns}$$

The diameters from equation 1 and 2 obtained are 13 cm and 14 cm respectively. The original dimension of the object was 17cm.

### **Survey 3:**

Survey3 has been done longitudinally in the space where the concrete cylinder was buried as shown in Figure 3.42, in order to determine its length. There was a disturbance along the length where the block was present as shown in Figure 3.44. From the radargram the length can be approximately assessed as 2.5cm which is equal to the original length.

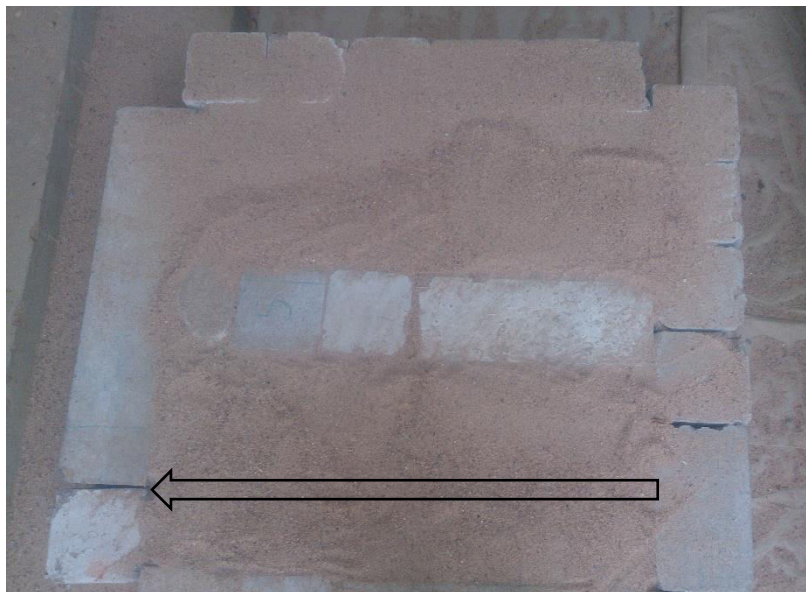


**Fig.3.42:** Test-pit with direction and location of test

1. DAT\_0394\_B1.RD3 / traces: 207 / samples: 384

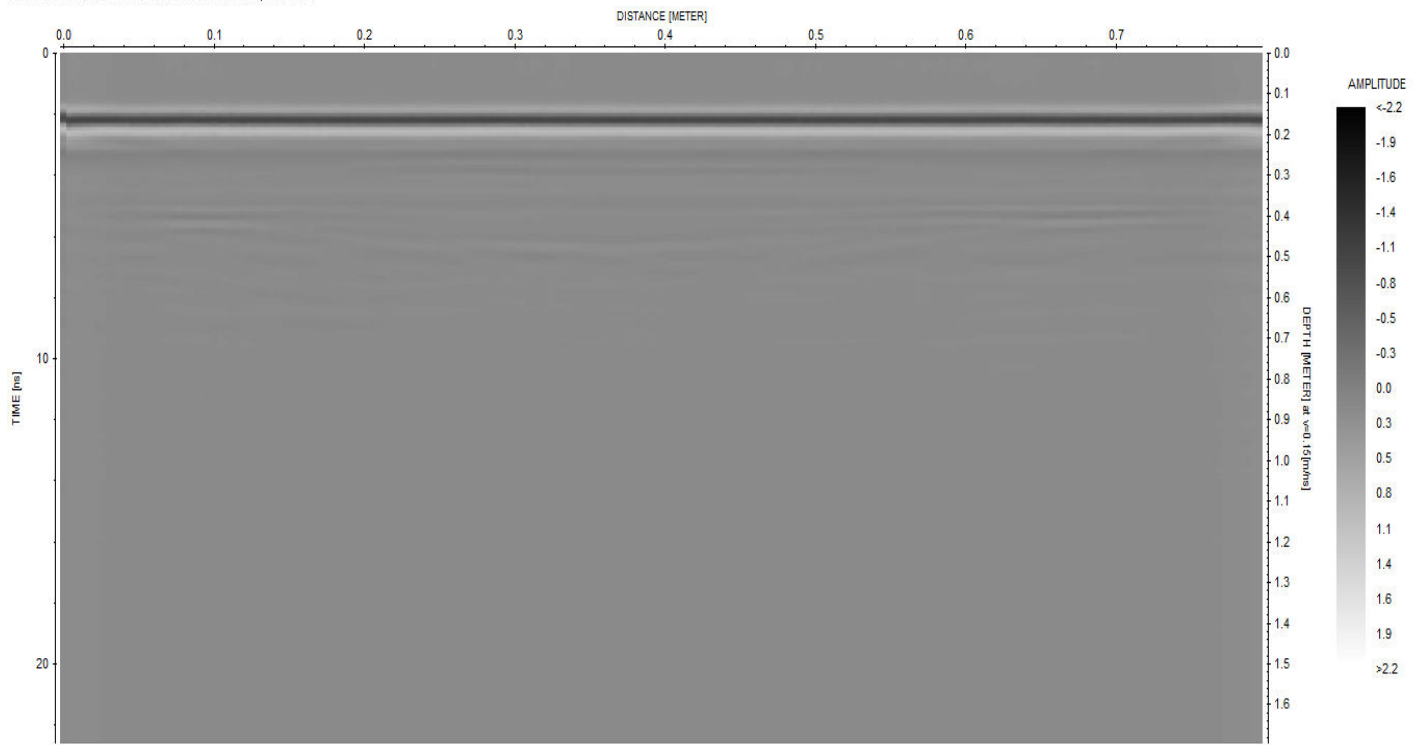


**Fig.3.43:** Unprocessed radargram

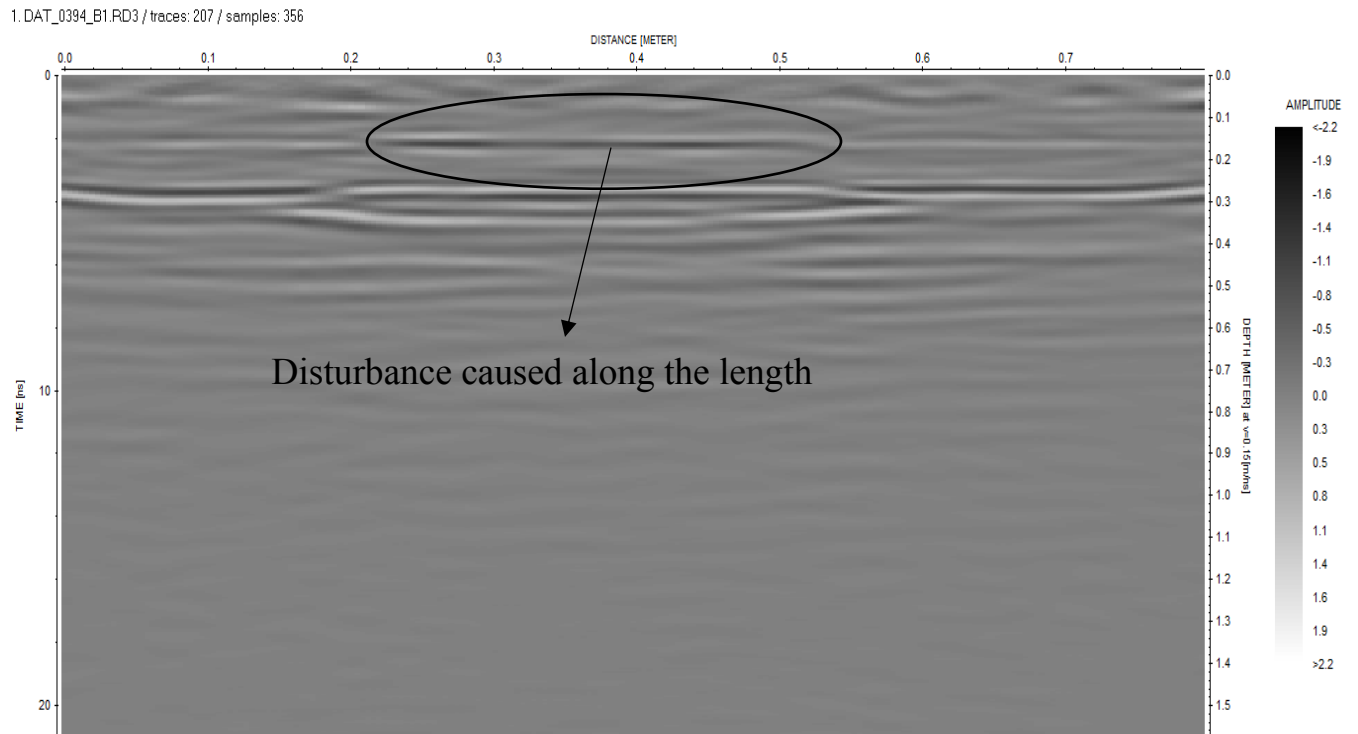


**Fig.3.44:** Processed radargram with identified disturbance

#### Survey 4:

Test 4 has been done longitudinally where the nearly rounded stone has been placed as shown in Figure 3.45. There was a hyperbolic reflection even longitudinally since it is rounded in shape as shown in Figures 3.46, 3.47 and 3.48. The hyperbolic fitting technique is used to determine its length, even in this direction.

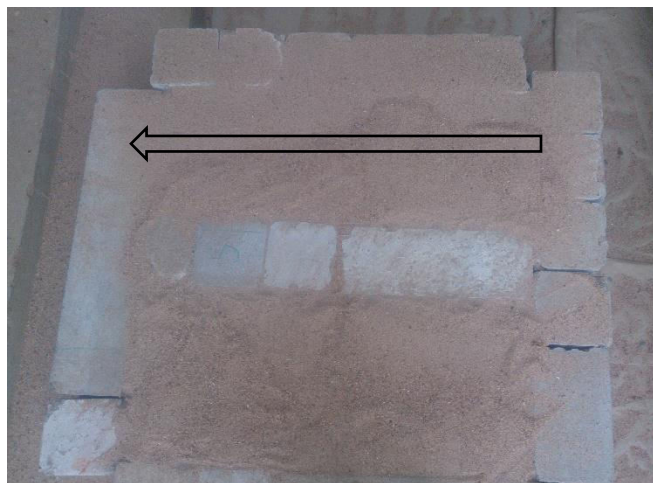




**Fig.3.45:** Test-pit with direction and location of test

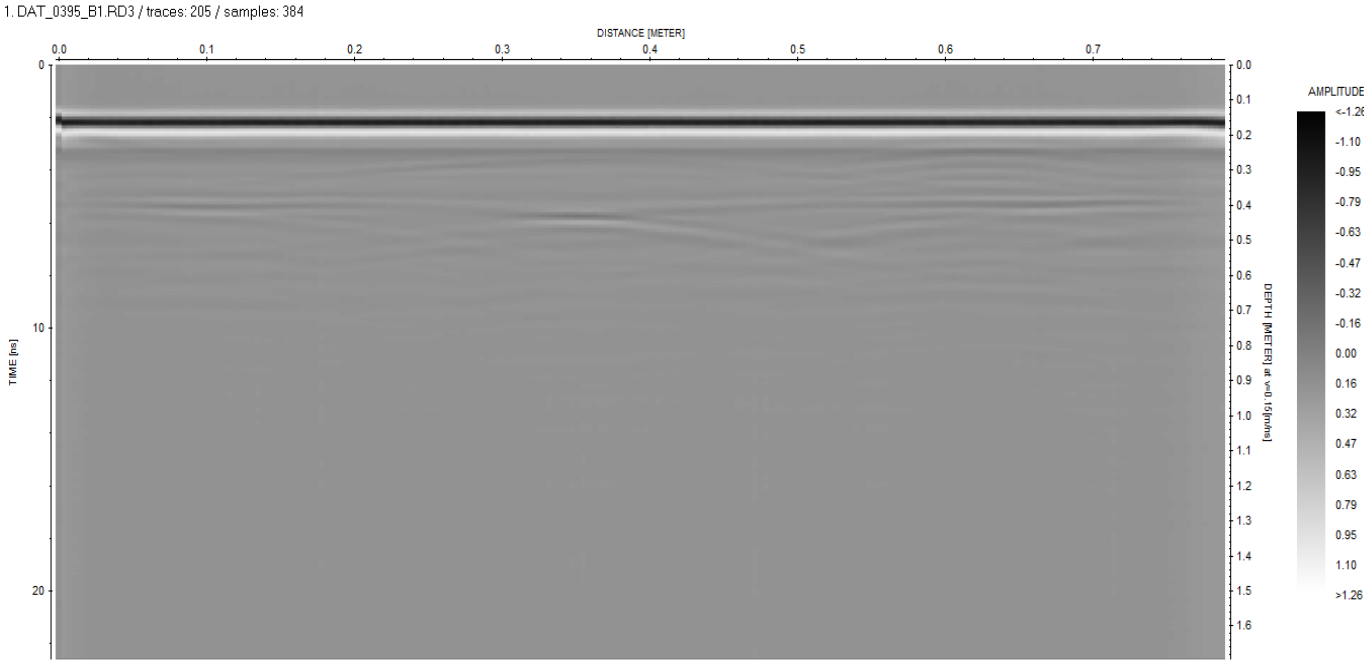


**Fig.3.46:** Unprocessed radargram

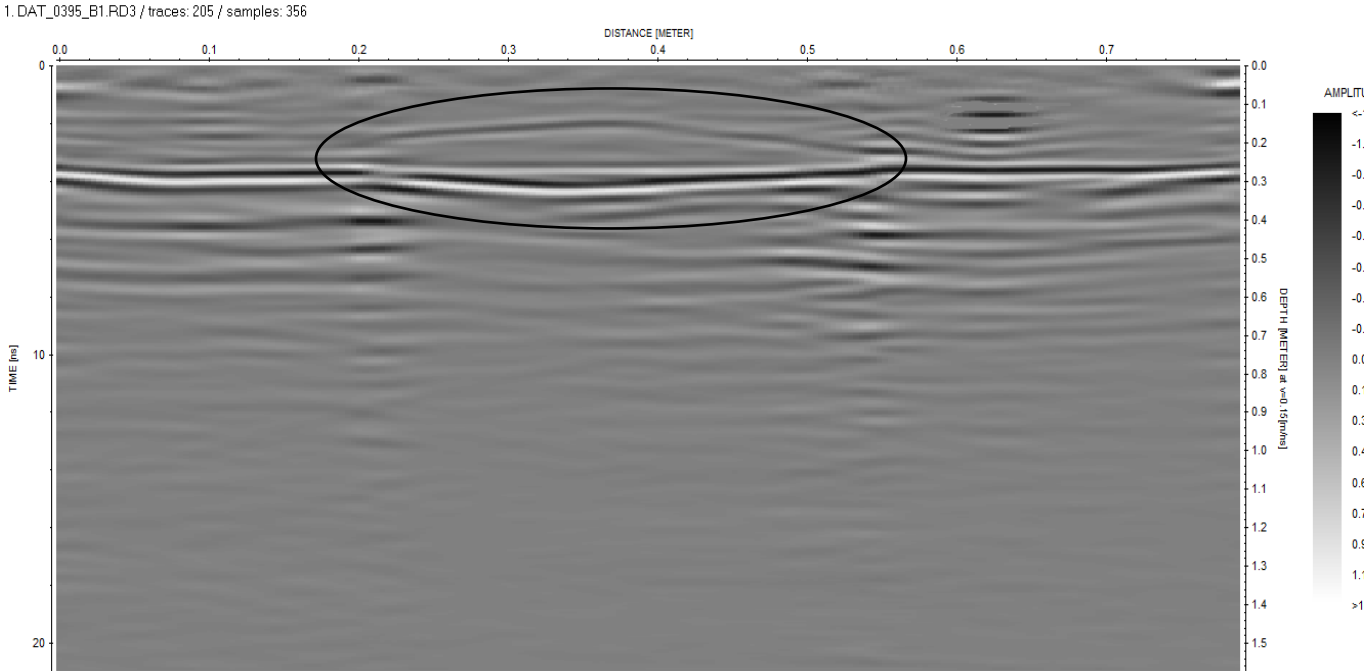


**Fig.3.47:** Processed radargram with hyperbolic reflection

1. DAT\_0395\_B1.RD3 / traces: 205 / samples: 356

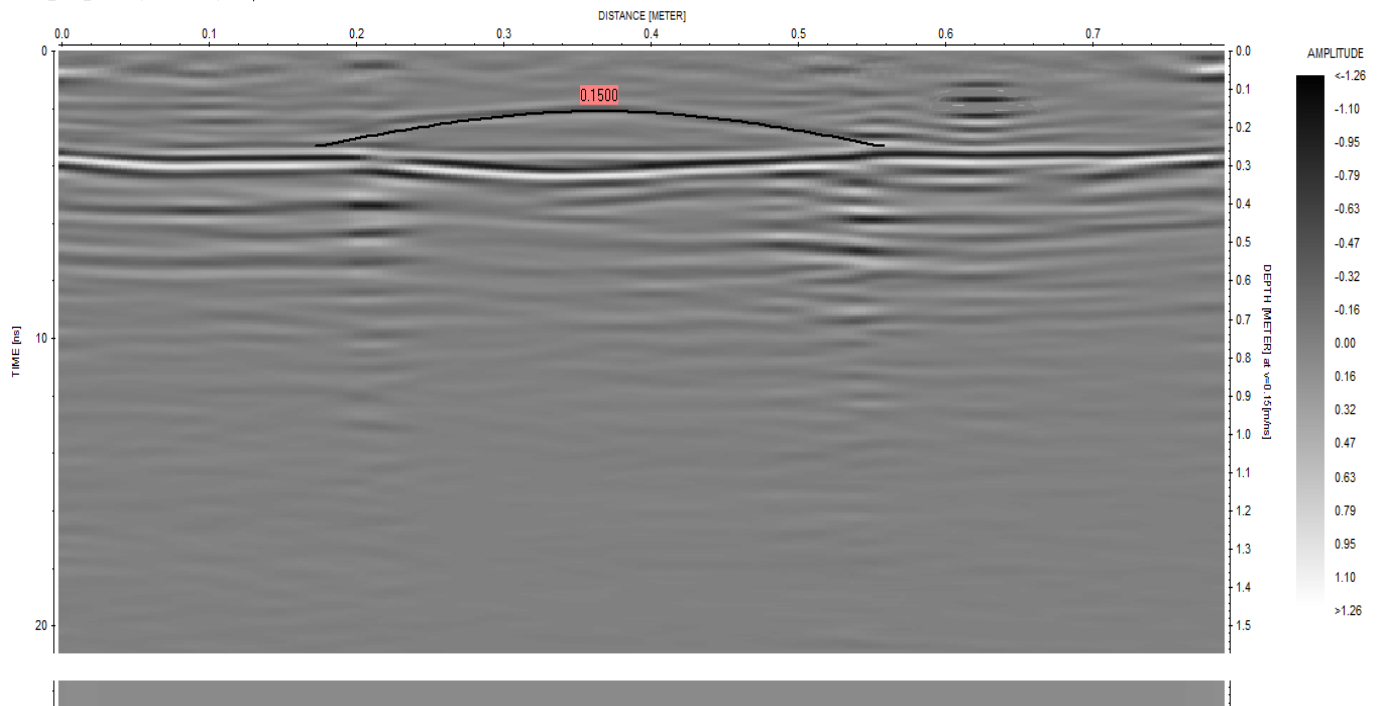


**Fig.3.48:** Processed radargram with hyperbola fitting

**Diameter of stone in longitudinal direction:**

$$a = t_0 + \frac{2R}{v} \dots\dots\dots(1)$$

$$b = \frac{v}{2} (t_0 + \frac{2R}{v}) \dots\dots\dots(2)$$

a=2.7

b=0.21

v=0.15 m/ns

t<sub>0</sub>= 1.9ns

The diameters from equation 1 and 2 obtained are 11 cm and 11.5 cm respectively. The original dimension of the object was 13cm.

### Survey 5:

Test 5 has been done along the test 2 direction, however, started from the concrete boundary on either side of the test pit as shown in Figure 3.49. The difference in materials from concrete to sand and to concrete again could be clearly distinguished from the radargram as shown in Figure 3.50 and 3.51.

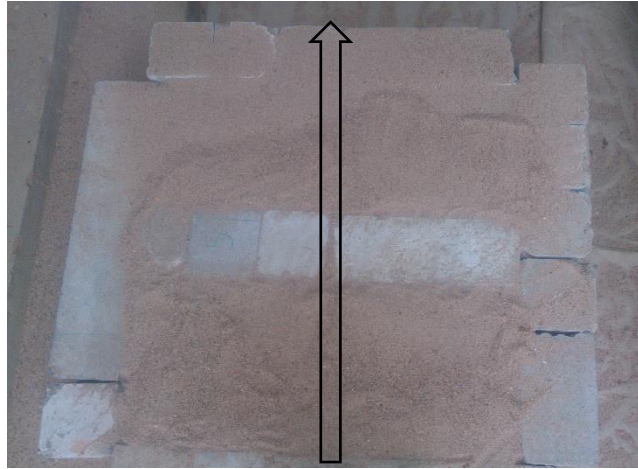


**Fig.3.49:** Test-pit with direction and location of test

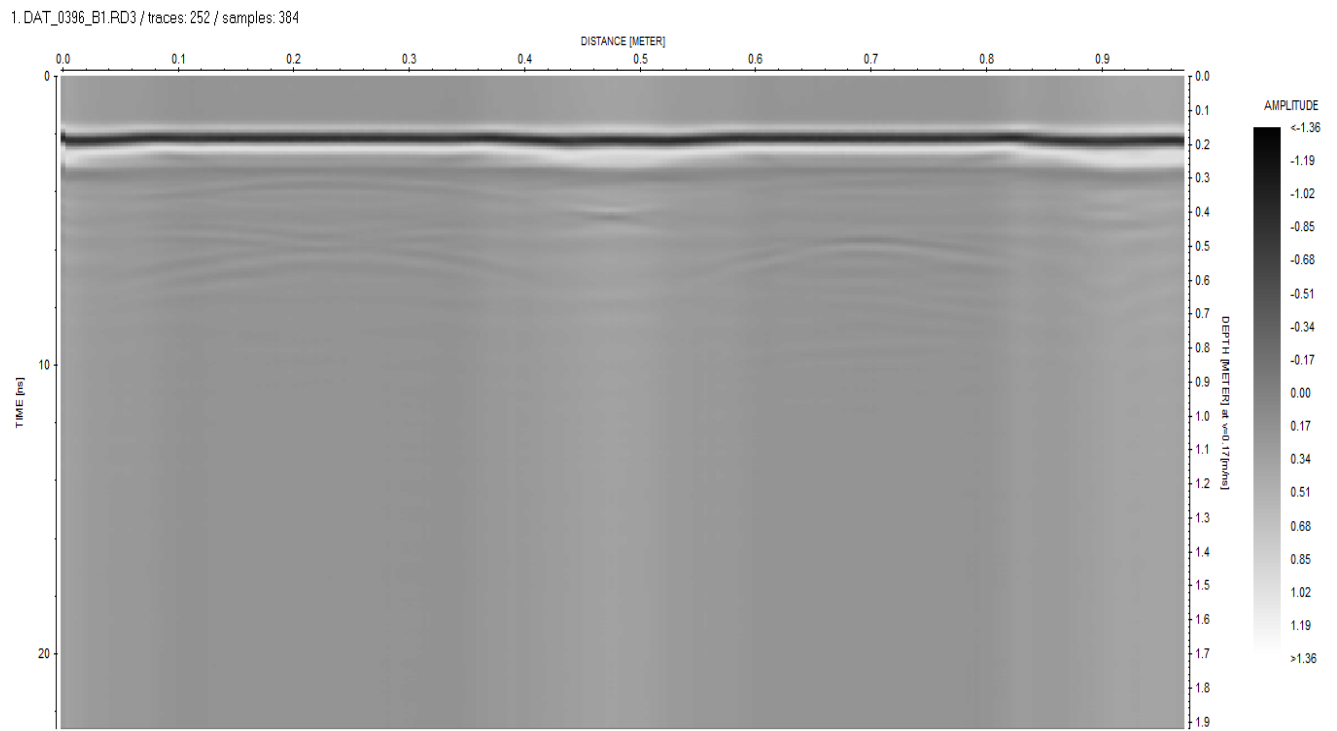


**Fig.3.50:** Unprocessed radargram

1. DAT\_0396\_B1.RD3 / traces: 252 / samples: 356

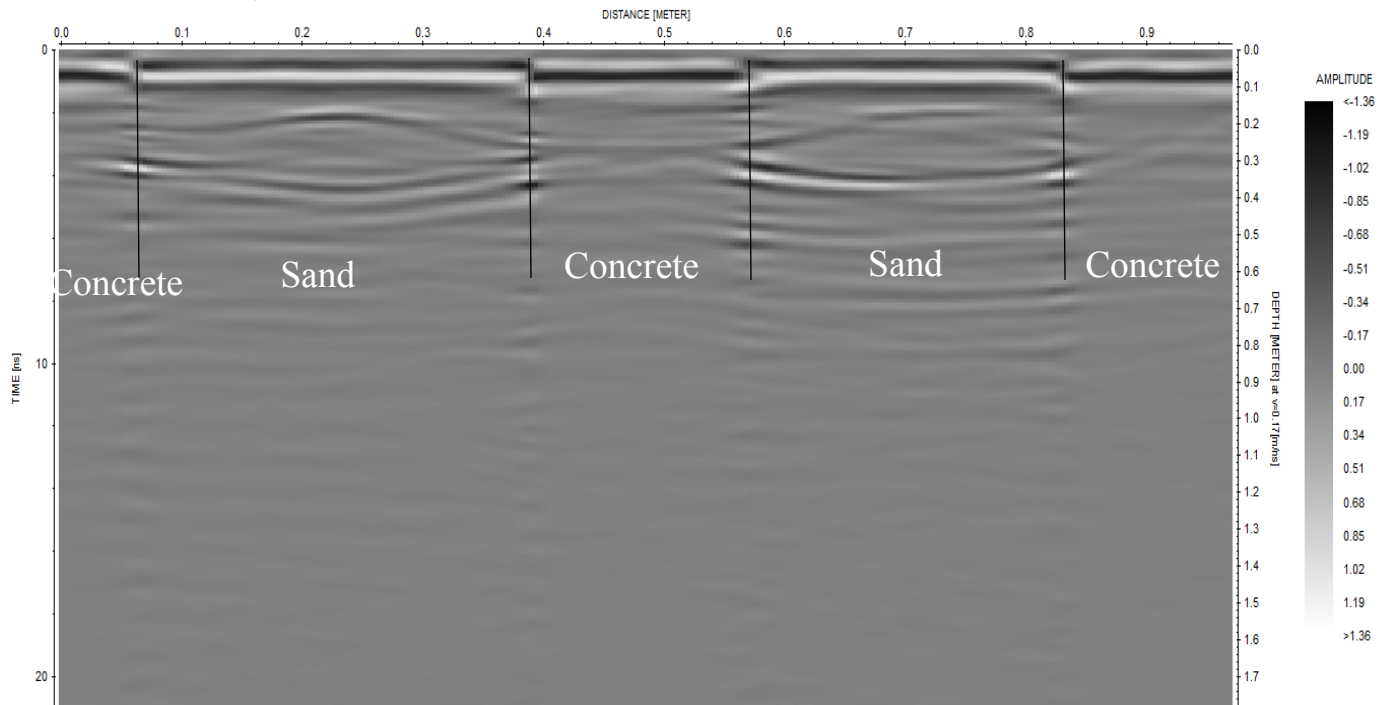


**Fig.3.51:** Processed radargram with all the areas differentiated

### Summary:

- The calibration studies gave insight about the radargrams produced with 1.6 GHz GPR antenna on RC slab and calibration sand test-pits. A clear demarcation between the well compacted and poorly compacted soils could be identified.
- The calibration of 500 MHz was done on a clay test-pit.
- The radargrams are more prominent in case of metal objects when compared to other objects or materials.
- The diameter of the objects identified using GPR have been successfully determined using hyperbolic fitting technique with a very minimal error.

## Chapter 4

# Determination of Soil Deformations under Bridge Approach Slabs

## 4.1 Introduction

The GPR technique is used in the determination of sub soil deformations under bridge approach slabs over a stretch selected on NH-9 near Outer Ring Road cross at Patancheru, Hyderabad. The Google image of the test stretch of GPR survey is shown in Figure 4.1. The particular stretch is selected since the approach slabs on the west and east sides have settled. The GPR testing has been done and the areas of soil deformations has been identified. The survey has been done using a 500 MHz antenna over a length of stretch 100m. Various surveys have been done from both the directions on the pavement stretch i.e. from West to East (Vijayawada to Pune) and vice versa. Also LWD tests were done at particular intervals on the selected stretch to validate the data.

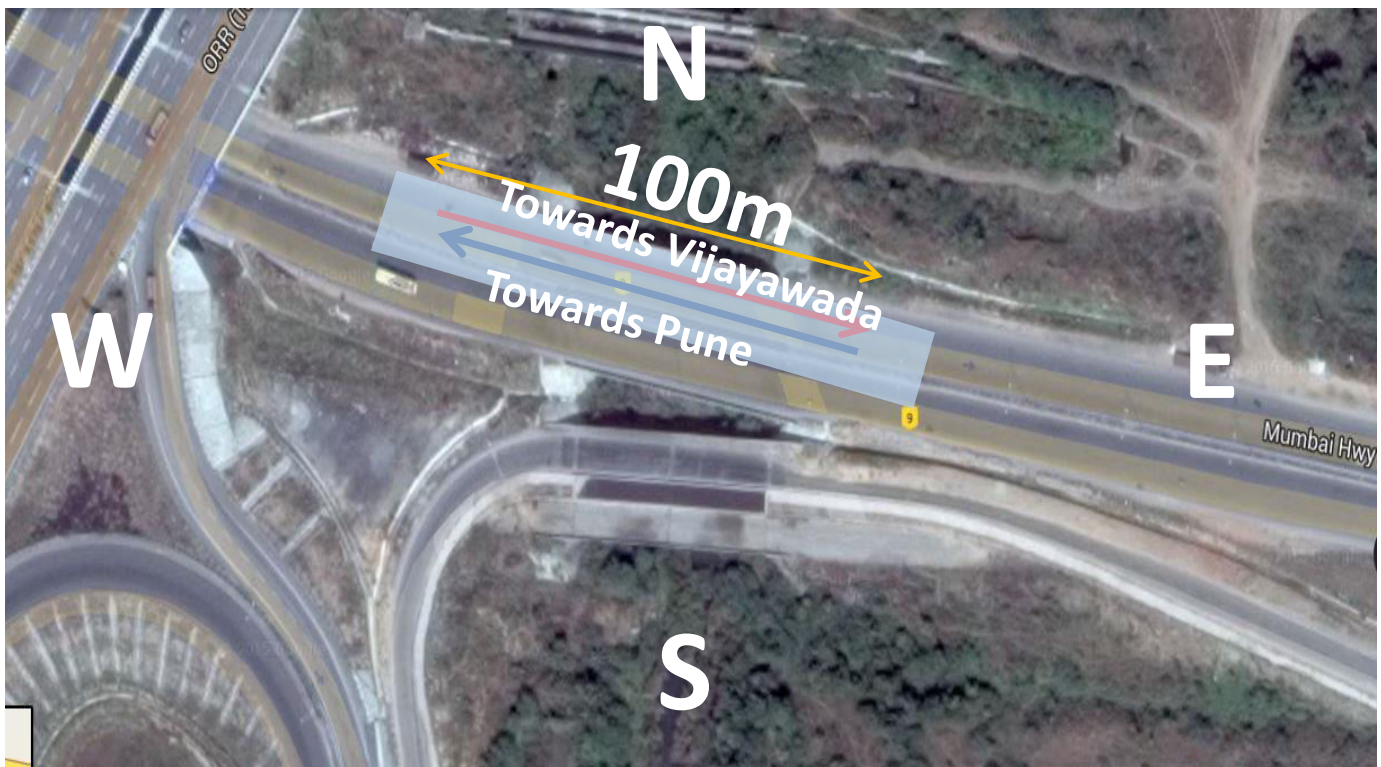


**Fig.4.1:** Google Image of the Bridge Site near Outer Ring Road, Hyderabad

## 4.2 Description of the Bridge Approach site

The national highway (NH 9) and the bridge section is oriented east-west directions as shown in the Figure 4.2. A 100 m test section covering undisturbed pavement sections on either side of the approach

embankments, zones covering settled approach slabs and the firm bridge section were considered for the GPR surveys. From 0m to 17m, covers the undisturbed approach embankment portion. The approach slab on the west side starts from 17m and ends at 21.5m. The stretch of approach slab from 20m to 21.5m rests on the wing wall and the bridge abutment and the remaining length rests over the embankment soil. The bridge deck spans from 21.5m to 78.5m with three expansion joints present at 21.5m, 50m and 78.5m. The whole stretch is symmetrical about the centrally located expansion joint as shown in Figure 4.2. The markings shown in the Figure 4.2 represent the corresponding chainages and can be seen in the GPR surveys as well. markings done in the GPR while doing the survey. Figures 4.3 to 4.6 shows the visuals of the bridge approach site. Along the GPR survey track, light weight deflectometer (LWD) testing are carried out to verify/quantify the modulus of the test sections.

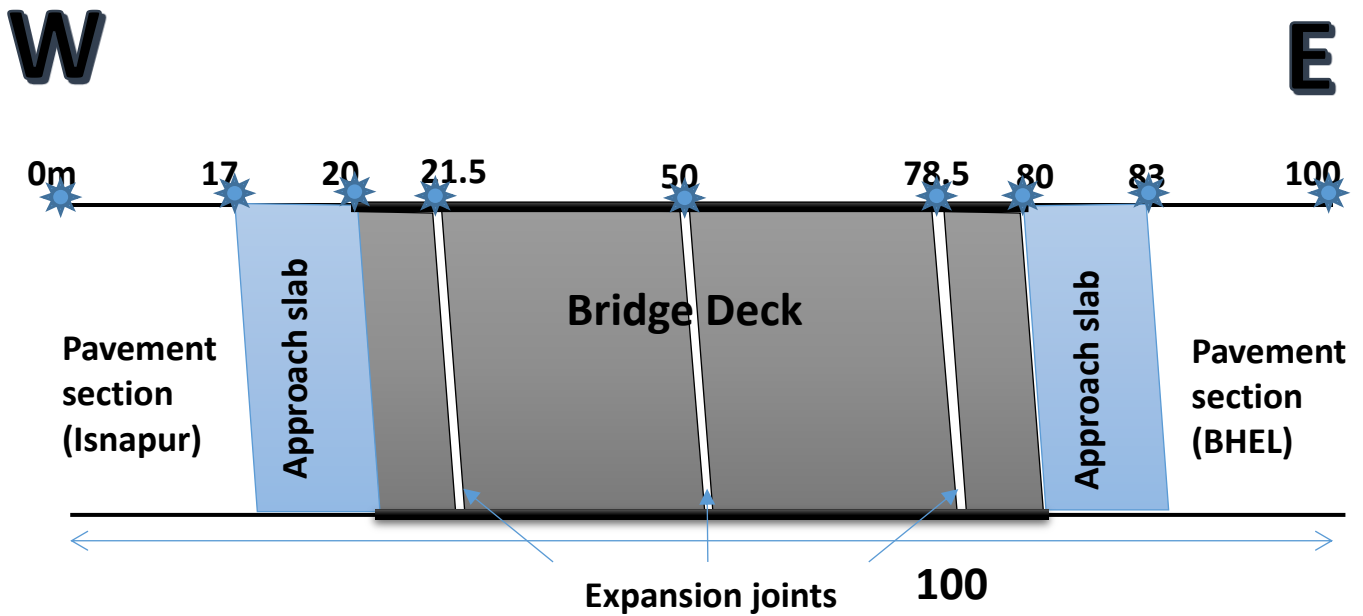


**Fig.4.2:** Plan view of the Bridge approach



**Fig.4.3:** Stretch of the pavement on which survey was done



**Fig.4.4:** View showing the approach slab, wing wall and bridge deck



**Fig.4.5:** GPR testing on the pavement



**Fig.4.6:** LWD testing on the pavement

### 4.3 GPR Survey

#### **Survey 1: Complete stretch from 0m to 100m (West to East direction)**

Survey 1 was done on the whole stretch from 0m to 100m (West to East) with a radar wave velocity of 0.14m/ns. While surveying, markings were done at chainages as shown in Figure 4.2. The obtained data was post-processed in the software and the radargrams were analyzed to check for any soil deformations. There was a kink throughout the depth at the location of expansion joints i.e. at 21.5m, 50m and 78.5m as can be seen in figure 4.8. The approach slab area and the bridge deck spanning from 17m to 83m showed strong reflection compared to other areas owing to the fact that it is concrete material as can be seen in figure 4.8. There were soil deformations identified in the stretch from 15m to 17m and 83m to 91m at a depth of approximately 1m from ground surface. The deformation in the stretch 83m to 91m were identified to be more compared to the latter case. The volume of the soil deformation in both the cases have been calculated per lane width and obtained to be  $0.14\text{m}^3/\text{lane}$  in the 15m to 17m stretch and  $0.805\text{m}^3/\text{lane}$  in the 83m to 91m stretch. Also a settlement of 0.03m has been identified in the pavement section from 0m to 17m as compared to that of bridge section.



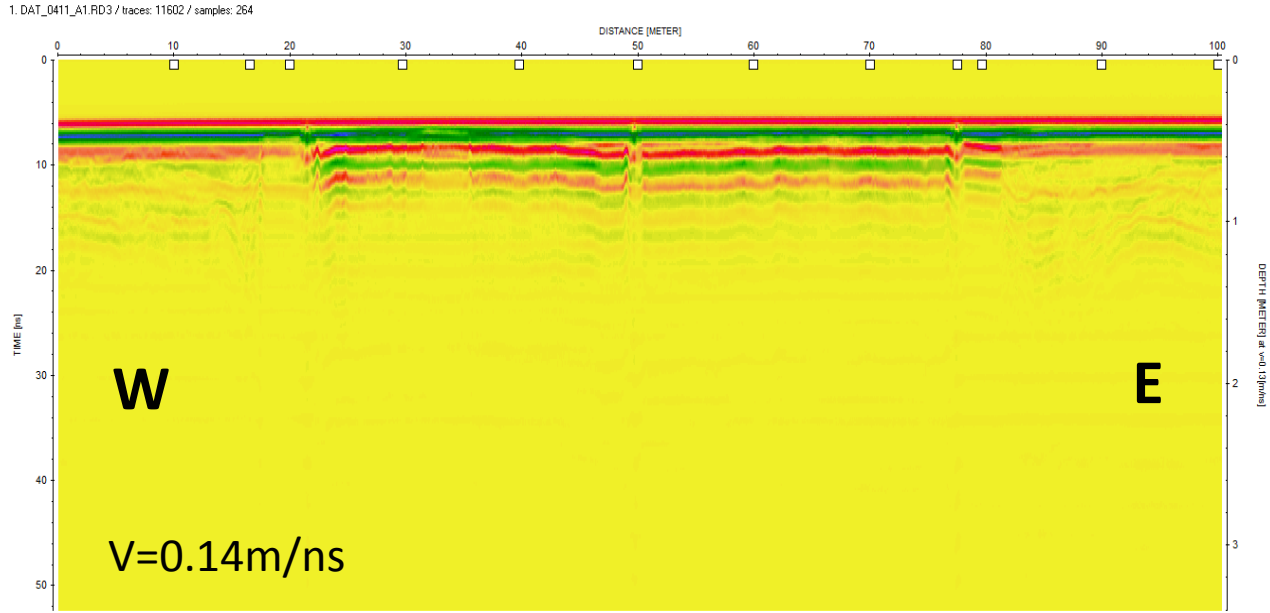


**Fig.4.7:** Unprocessed radargram from 0m to 100m (West to East)

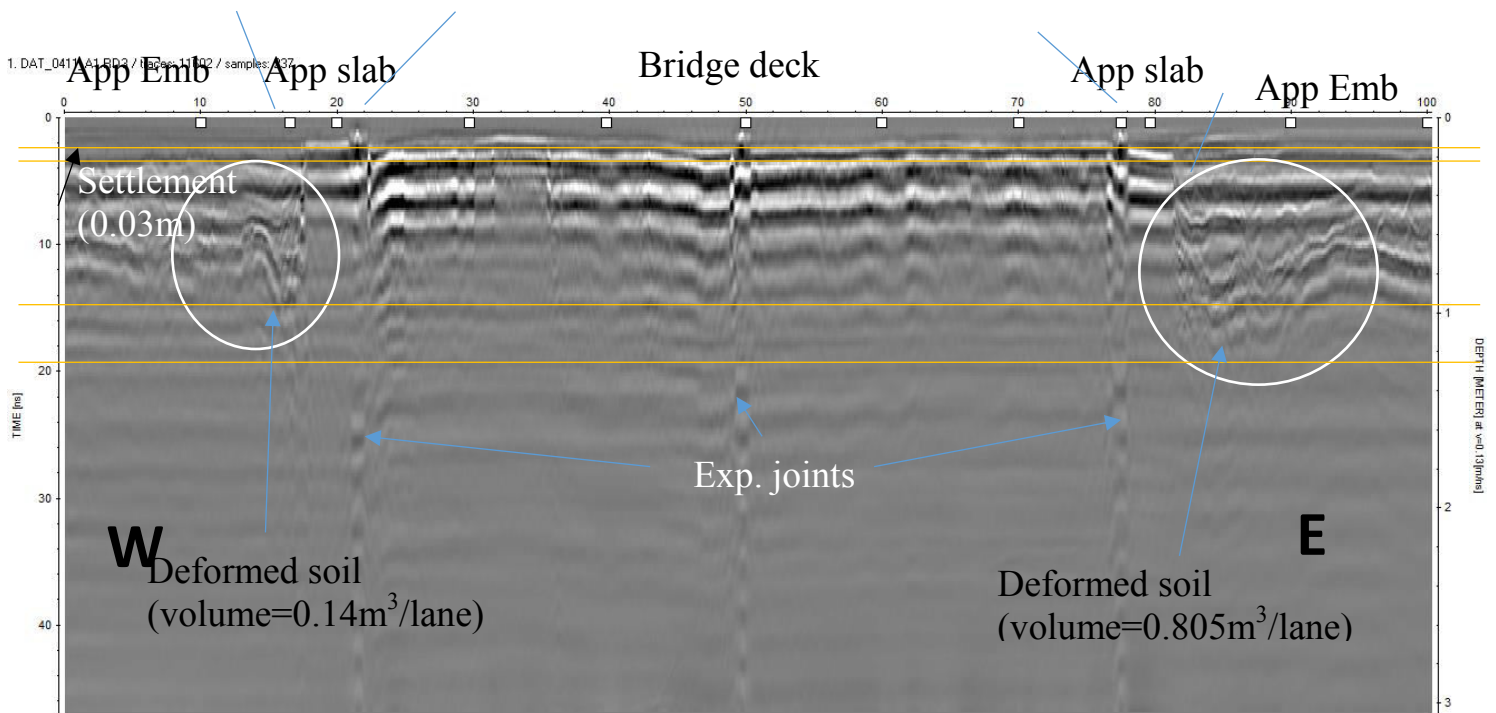


**Fig.4.8:** Processed radargram from 0m to 100m (West to East)

### Survey 2: Complete stretch from 100m to 0m (East to West direction)

Survey 2 was done on whole stretch from East to West direction changing the radar wave velocity to 0.13m/ns to ensure that the data obtained in the Survey 1 was accurate. The radargram was showing similar kinks and deformations at the same chainage locations as in the previous case as can be seen in Figure 4.10.

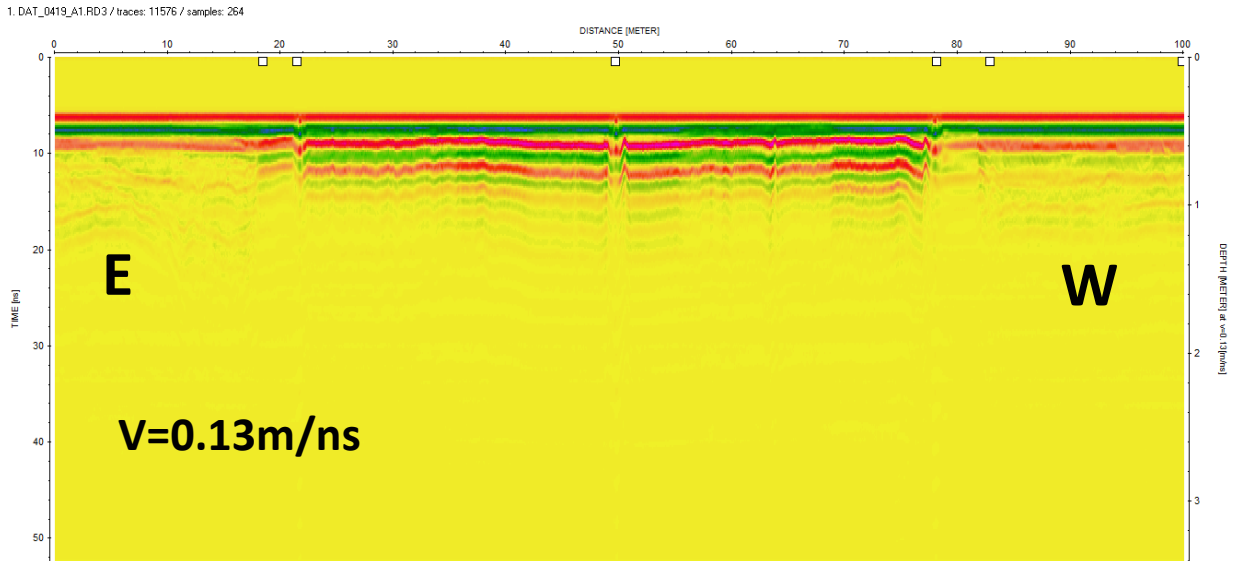


Fig.4.9: Unprocessed radargram from 100m to 0m (East to West)

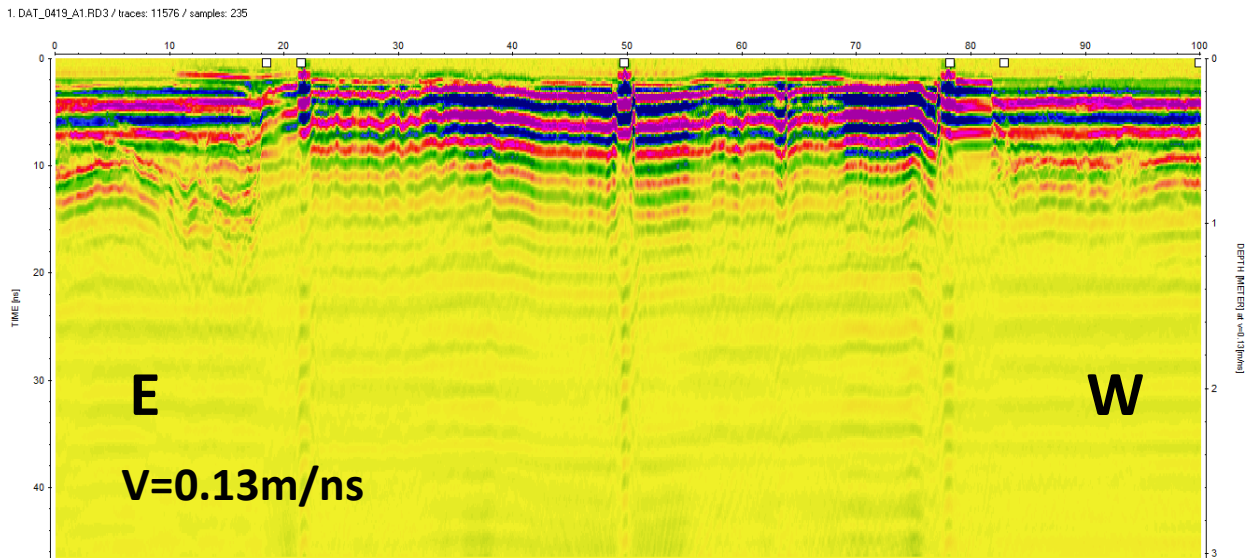


Fig.4.10: Processed radargram from 100m to 0m (East to West)

### Survey 3: Complete stretch from 0m to 100m (West to East) Trial 2

Survey 3 was run again from 0m to 100m i.e. from West to East direction, but with a changed radar wave velocity of 0.14m/ns to observe if any changes occur in the radargrams. The radargram after post processing did not show any considerable changes as compared to that of survey 1, and also the deformations and disturbance locations were matching were with that of survey 1. Hence the survey results are repeatable and validated.

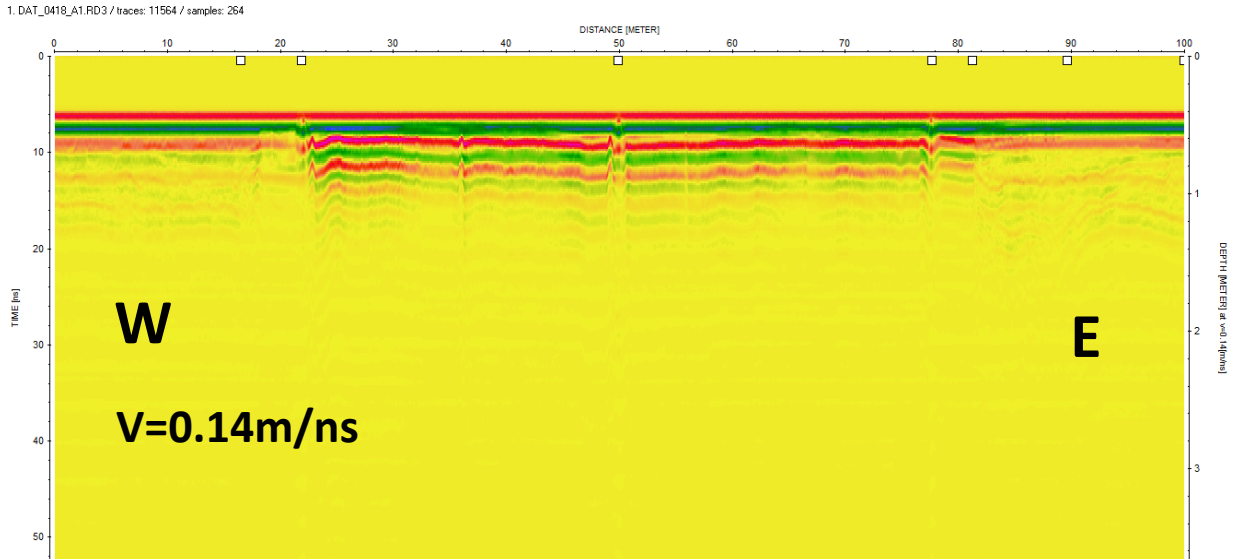


Fig.4.11: Unprocessed radargram from 0m to 100m

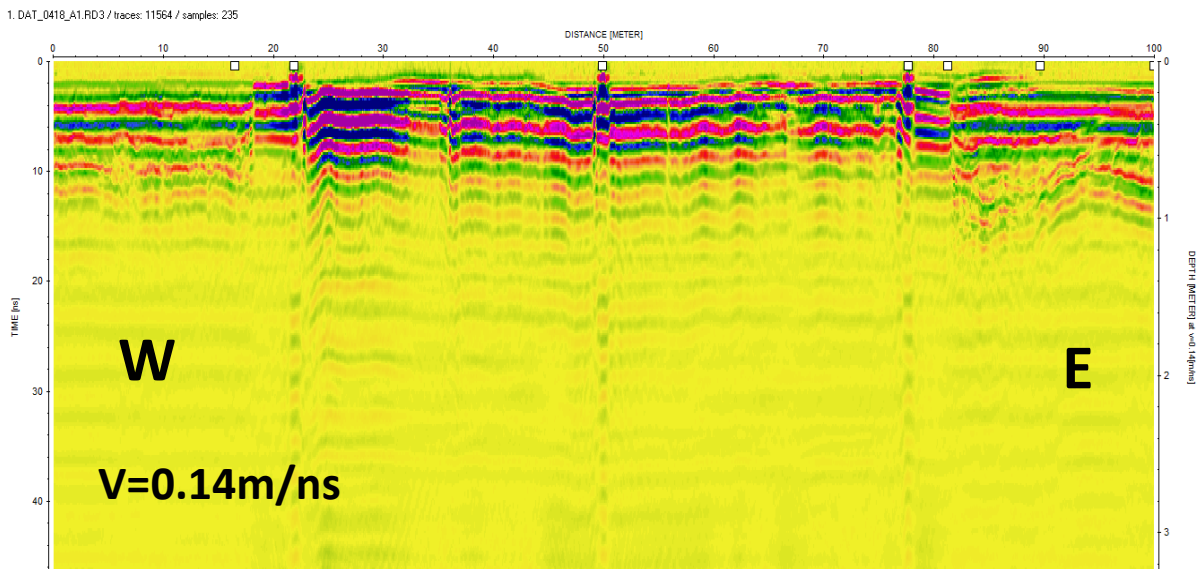


Fig.4.12: Processed radargram from 0m to 100m

### Survey 4: Stretch from 100m to 78.5m (East to West direction)

Survey 4 was done from 100m to 78.5m i.e. from East to West direction with a radar wave velocity of 0.14m/ns to clearly visualize the deformations under the pavement section adjacent to the approach slab at a larger scale. There was a settlement of the soil observed just adjacent to the approach slab as can be seen in Figures 4.14 and 4.15, because of this settlement at this particular stretch there was a pavement layer overlain above the existing one as can be seen in Figure 4.5.

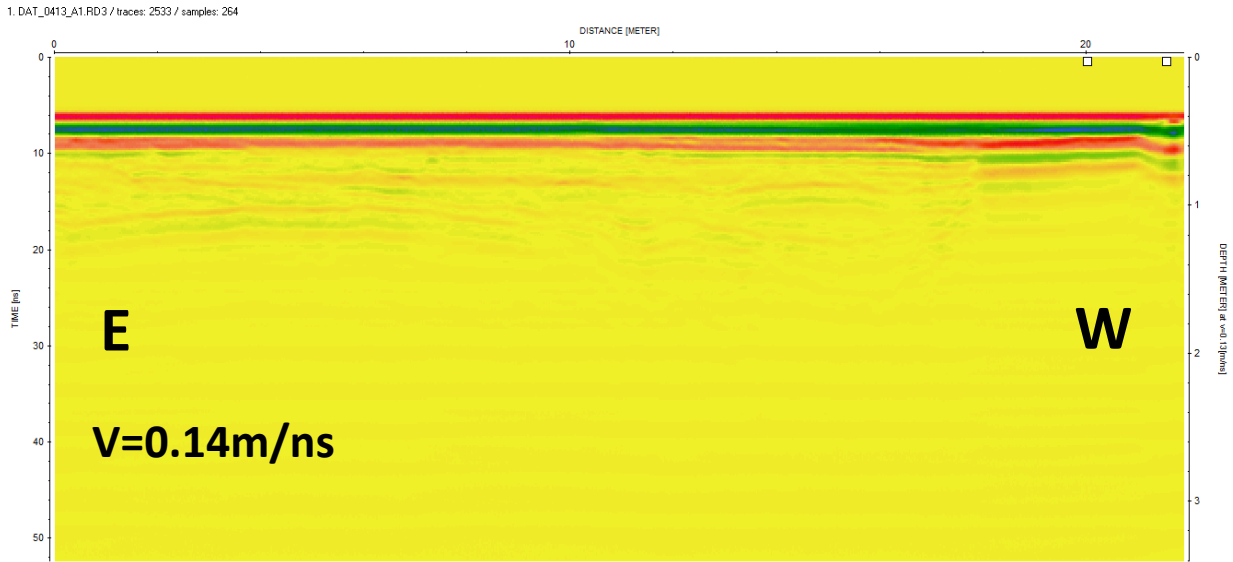


Fig.4.13: Unprocessed radargram from 100m to 78.5m

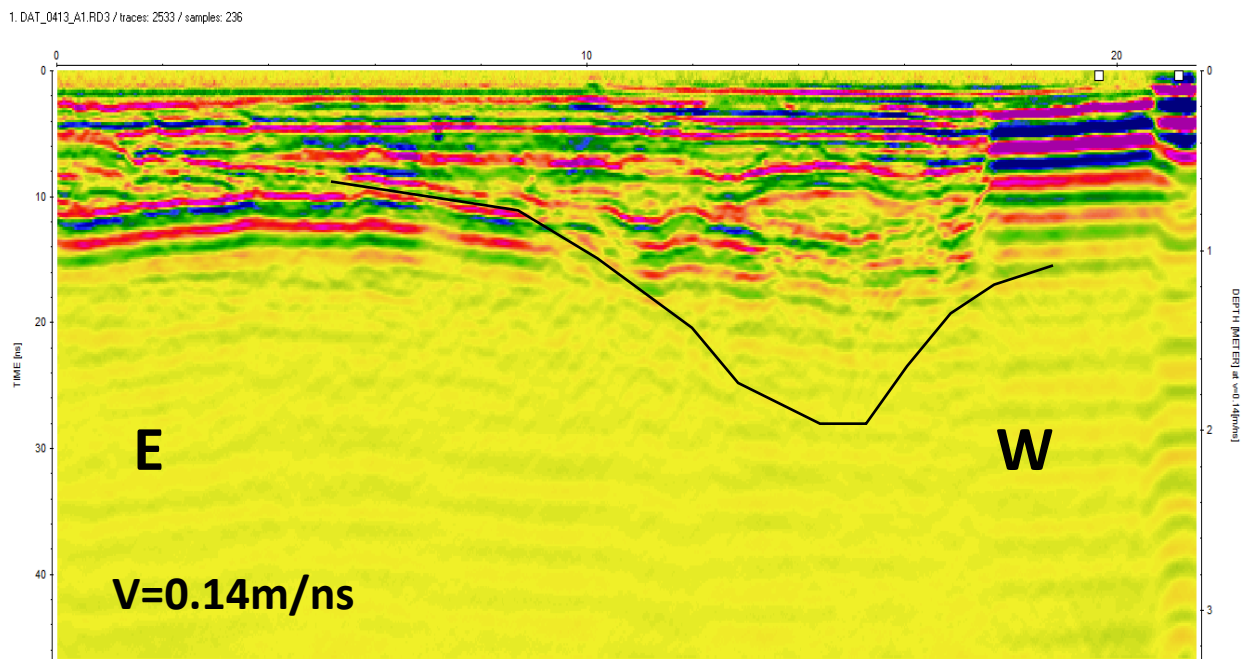
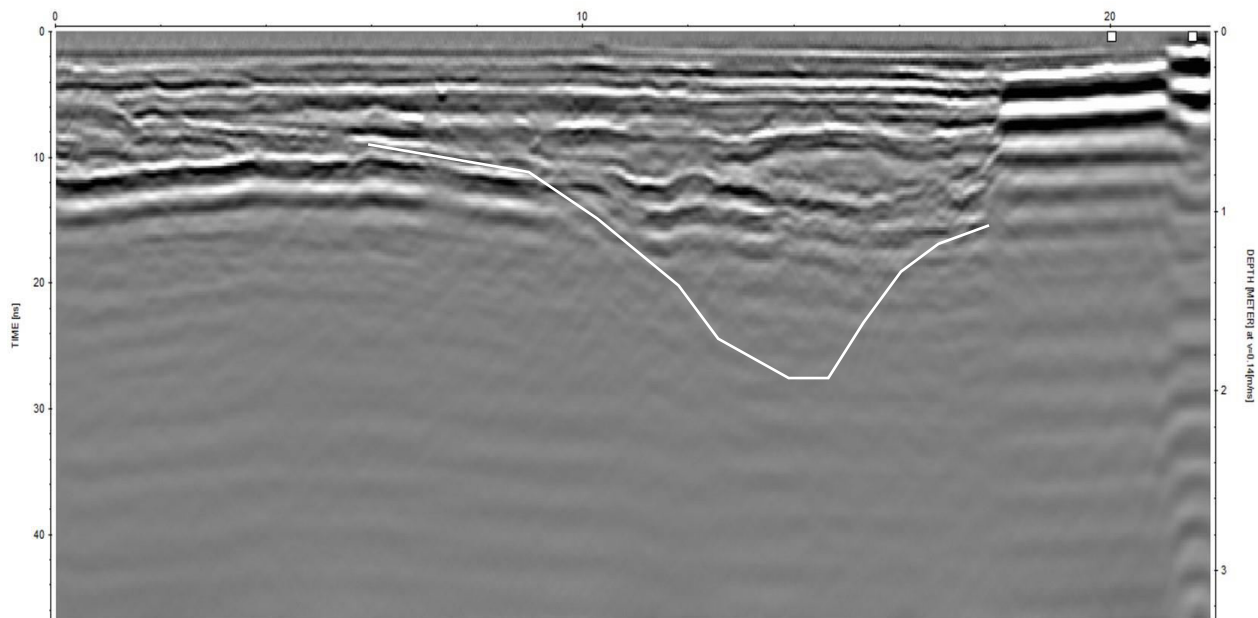


Fig.4.14: Processed Radargram from 100m to 78.5m



**Fig.4.15:** Processed Radargram from 100m to 78.5m (Grey colored palette)

#### **Survey 5: Stretch from 78.5m to 21.5m (East to West direction)**

Survey 5 was conducted in the bridge deck section from 78.5m to 21.5m i.e. from first expansion joints to the third one in the direction East to West with a radar wave velocity of 0.12m/ns. At 0m, 28m and 57m where expansion joints were present disturbance all through the depth is present as can be seen in Figure 4.17.

1. DAT\_0414\_A1.RD3 / traces: 6610 / samples: 264

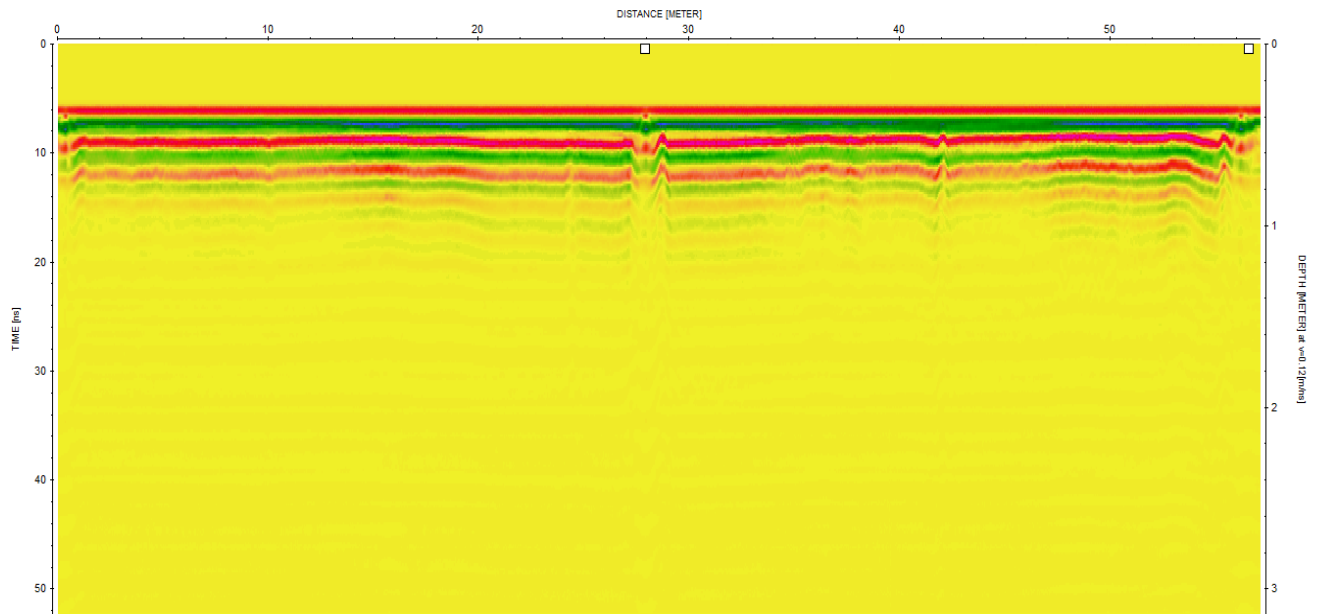


**Fig.4.16:** Unprocessed radargram from 78.5m to 21.5m

1. DAT\_0414\_A1.RD3 / traces: 6610 / samples: 236

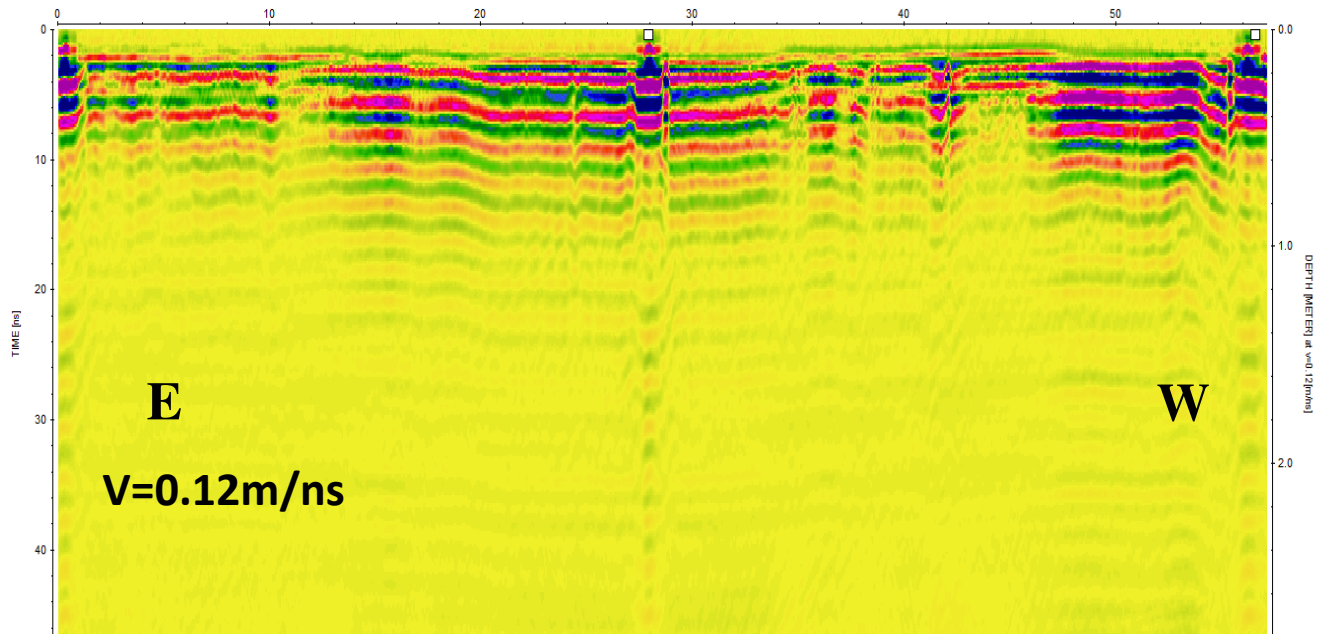


**Fig.4.17:** Processed Radargram from 78.5m to 21.5m

### Survey 6: Stretch from 21.5m to 0m (East to West direction)

Survey 6 was done from 221.5m to 0m in East to West direction to observe the deformations adjacent to approach slab in a larger scale. The soil compaction was identified to be weak adjacent to the approach slab as can be seen in Figures 4.19 and 4.20.

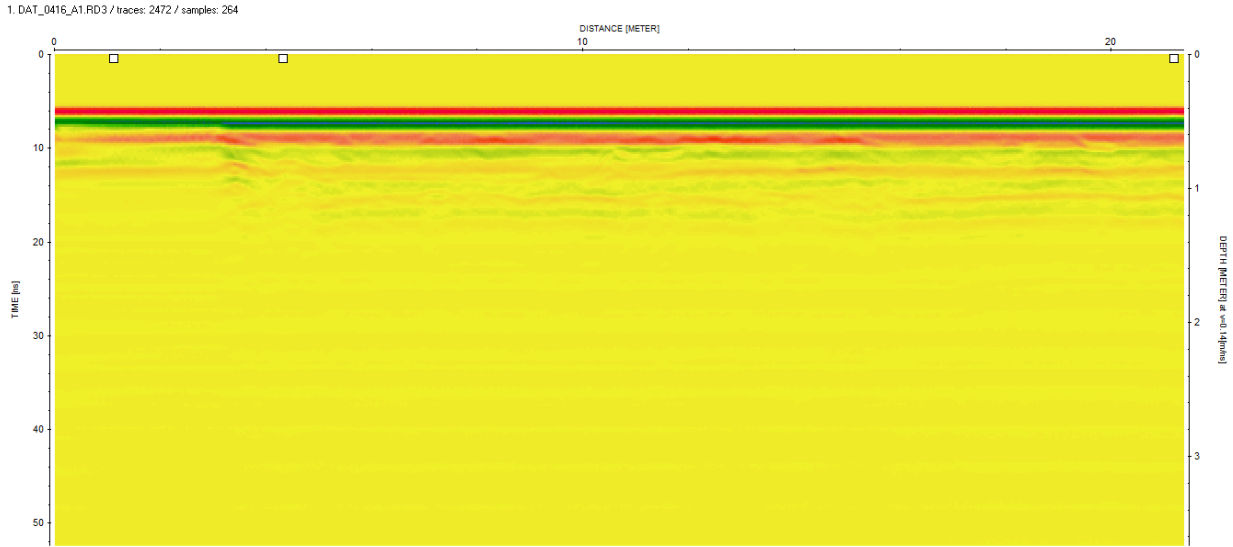


**Fig.4.18:** Unprocessed radargram from 21.5m to 0m

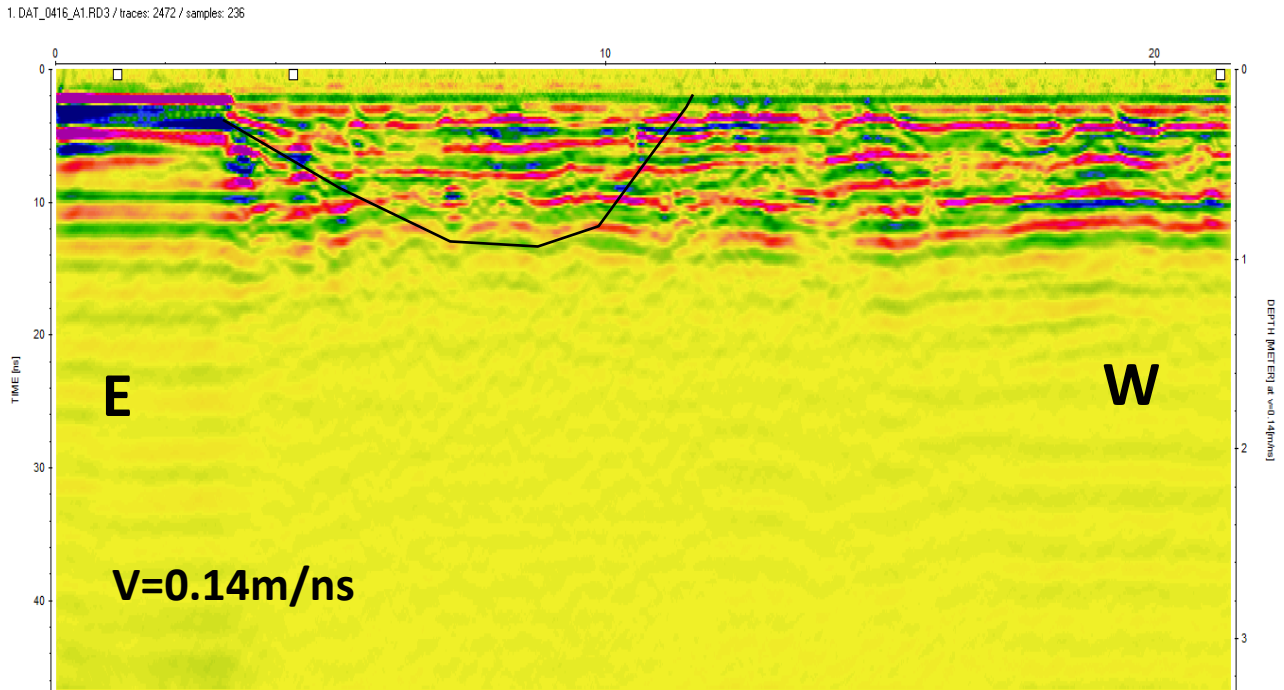


**Fig.4.19:** Processed Radargram From 21.5m to 0m

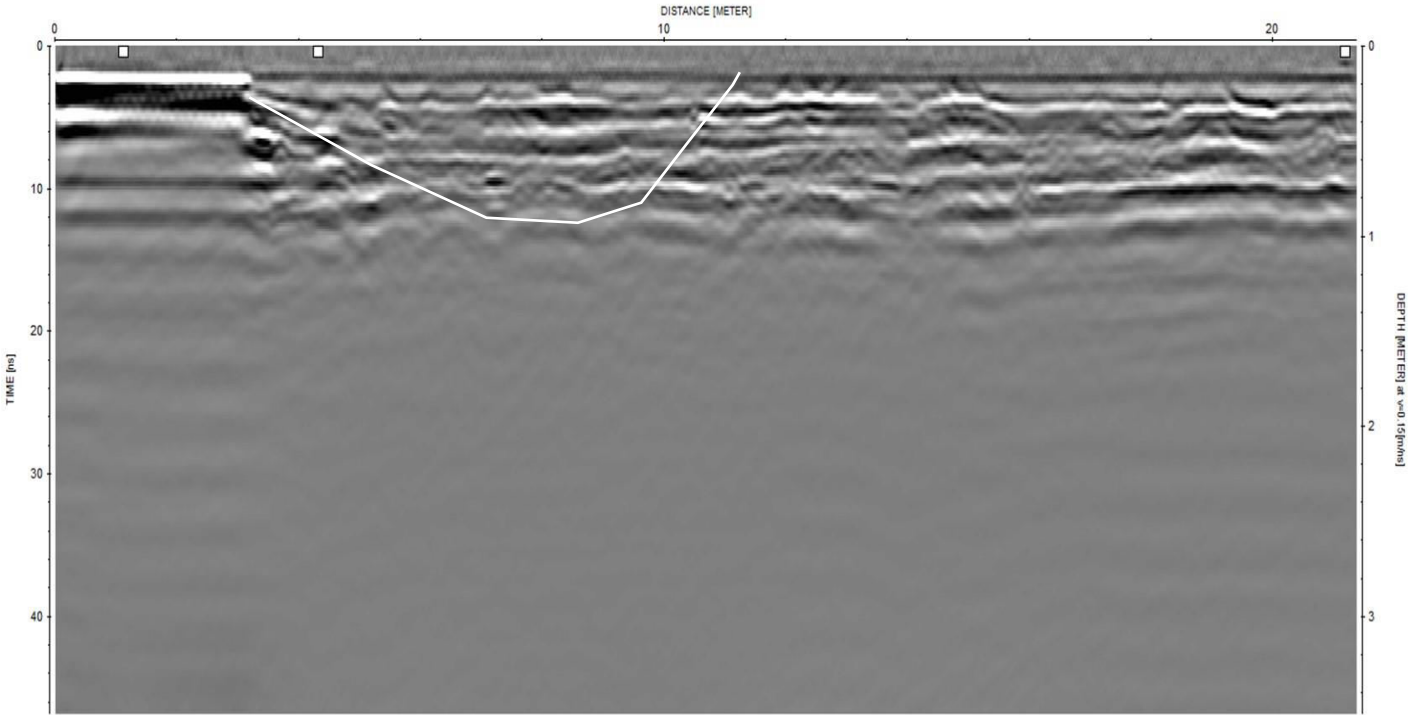


**Fig.4.20:** Processed Radargram from 21.5m to 0m (Grey colored palette)

#### 4.4 Deformation Modulus of the Pavement Sections

Light weight deflectometer (LWD) testing has been done on the pavement at chainages 0m, 15m, 25m, 75m, 85m, 100m and the deflections and deformation modulus values have been obtained. The LWD data is shown in the Table 4.1. It was observed that the deformation modulus was high i.e. 271.08 MPa and 284.81 MPa at 0m and 100m respectively where there were no soil deformations identified in the GPR radargrams. Adjacent to the approach slab, where severe deformations were identified in the radargrams, very low deformation modulii were recorded i.e. 135.5 MPa and 132.4 MPa at 15m and 85m respectively. On the stretch of bridge deck deformation modulii were recorded as 218.45 MPa and 220.35 MPa at 25m and 75m respectively, where there are no deformations identified in the radargram thus validating the GPR analysis.

Chainage (m)	D1 (mm)	D2 (mm)	63 D3 (mm)	Davg (mm)	Deformation modulus (MPa)
--------------	---------	---------	------------	-----------	---------------------------



0	0.085	0.083	0.081	0.083	271.08
15	0.165	0.173	0.16	0.166	135.54
25	0.098	0.103	0.108	0.103	218.45
75	0.101	0.106	0.108	0.105	220.35
85	0.157	0.17	0.183	0.17	132.35
100	0.077	0.079	0.081	0.079	284.81

**Table 4.1:** LWD test data

### **Summary**

GPR technique has been successfully adopted in determining the soil deformations under bridge approach slabs and also the deformations have been quantified to the nearest extent. As a validation LWD testing

has been done and the areas where deformations have been identified in the radargrams the deformation moduli were recorded to be very low.

## Chapter 5

### Conclusions

Various surveys have been conducted using GPR and also it has been used in assessing the condition of soil under Bridge approach slabs. The following are a few conclusions drawn from the research.

1. The Reinforcement details such as spacing, slab thickness, number of rebars located in the survey area, effective cover and also the diameter of rebar can be determined effectively with GPR analysis.
2. The diameter of solid circular objects can be determined to a good accuracy by hyperbolic fitting method.
3. GPR is a very effective tool in identifying the underlying objects in the ground.
4. It is highly sensitive to moisture.
5. It doesn't give satisfactory results if different materials of similar dielectric properties are present.
6. The reflections given by metal surfaces are stronger than any other surface.
7. Also homogenous materials, which possess same dielectric properties gives good reflections as compared to non-homogenous materials.
8. The areas of higher compaction and lower compaction can be identified by analyzing the GPR radargrams.

9. The diameter of hollow pipes can be determined by using the two way travel time of the radar wave and the radar wave velocity.
10. The selection of antenna frequency depends on the depth of interest. The higher the depth of interest the lower should be the antenna frequency and vice-versa.
11. The direction of GPR survey is a very important criteria while analyzing the radargrams.
12. The reflections are good in case of densely packed materials than in case of loosely packed materials.
13. GPR is a very effective non-destructive technique in assessing the quality of pavements.
14. Soil deformations along with their depth and the area of location can be identified through analysis of GPR radargrams.

## References

1. Cardimona, S., (2007), "*Subsurface Investigation Using Ground Penetration Radar*," [http://www.dot.ca.gov/hq/esc/geotech/gg/geophysics2002/059cardimona\\_%20radar\\_overview.pdf](http://www.dot.ca.gov/hq/esc/geotech/gg/geophysics2002/059cardimona_%20radar_overview.pdf).
2. Maser, K. R., (2000), "*Pavement Characterization Using Ground Penetrating Radar: State of the Art and Current Practice*," Non-destructive Testing of Pavements and Back calculation of Moduli: Third Volume, ASTM STP 1375.
3. Chen, D-H, and Scullion, T., (2007), "*Detecting Subsurface Voids Using Ground-coupled Penetrating Radar*," Geotech. Test. J., Vol. 31, No. 3.
4. Al-Qadi, I. L., (1990), "*Detection of Moisture in Asphaltic Concrete By Microwave Measurements*," Ph.D. Thesis, The Pennsylvania State University, College Park, PA.
5. Hughes, C. S., Simpson, A. L., Cominsky, R., Pendleton, O. J., Weed, R. M., and Wilson, T., (1996), "*Measurement and Specification of Construction Quality, Volume 1L Final Report*," FHWA Report DTFH61-94-C-O0078, Brent Rauhut Engineering Inc., Austin, TX 78759.
6. Scullion, T. and Saarenketo, T., (2000), "*Integrating Ground Penetrating Radar and Falling Weight Deflectometer Technologies in Pavement Evaluation*," Non-destructive Testing of Pavements and Back calculation of Moduli: Third Volume, ASTM STP 1375, S. D. Tayabji and E. O. Lukanen, Eds., American Society for Testing and Materials, West Conshohocken, PA.

7. Chen, D-H, and Scullion, T., (2006), "Using Non-destructive Testing Technologies to Assist in Selecting the Optimal Pavement Rehabilitation Strategy," J. Of Testing and Evaluation, Vol. 35, No. 2.
8. Uddin, W., and Hudson, R., (1994), "Evaluation of NDT Equipment for Measuring Voids under Concrete Pavements," Non-destructive Testing of Pavements and Back calculation of Moduli (Second Volume]. ASTM STP 1198, Harold L. Von Quintas, Albert J. Bush, III, and Gilbert Y. Baladi, Eds., American Society for Testing and Materials, Philadelphia.
9. Leucci, G., and Negri, S., (2006), "Use of ground penetrating radar to map subsurface archaeological features in an urban area," Journal of Archaeological Science, 33(4), pp502–512.
10. Holt, E. B., and Eckrose, R. A., (1989), "Application of Ground-Penetrating Radar and Infrared Thermography to Pavement Evaluation," Non-destructive Testing of Pavements and Back calculation of Moduli, ASTM STP 1026, A. J. Bush III and G. Y. Baladi, Eds., American Society for Testing and Materials, Philadelphia, pp. 105-115.
11. Stolte, C. and Nick, K., (1994), "Eccentricity-migration: A method to improve the imaging of pipes in radar reflection data": Fifth International Conference on Ground Penetrating Radar, Ontario, Canada, Expanded Abstracts, Proceedings, p. 723–733.
12. Al-Nuaimy, W., Huang, Y., Nguyen, V., and Eriksen, A. 2001, "Automatic detection of hyperbolic signatures in ground-penetrating radar data": SPIE International Conference on Subsurface and Surface Sensing Technologies and Applications III, Cam Nguyen, Editor, San Diego, Vol. 4491, p. 327–335.
13. Chen, D. H., and Scullion, T. (2008). "Detecting subsurface voids using ground coupled penetrating radar." Geotech. Test. J., 31(3), 217–224. Daniels, D. J. (1996). Subsurface-penetrating radar, The Institute of Electrical Engineers, Los Alamitos, Calif., 1–62.
14. Chen, D. H., Nazarian, S., and Bilyeu, J. (2007). "Failure analysis of a bridge embankment with cracked approach slabs and leaking sand." J. Perform. Constr. Facil., 21(5), 375–381.
15. T. Saarenketo and T. Scullion, "Road evaluation with ground penetrating radar," Journal of Applied Geophysics, vol. 43, no.2–4, pp. 119–138, 2000.
16. Funk, T., Maierhofer, C., Leipold, S., and Borchardt, K. (1997). "Nondestructive location of tendon ducts in concrete for the installation of noise insulating walls using impulse radar." Proc., 7th Int. Conf. on Structural Faults and Repair, Vol. 2, M. C. Forde, ed., Engineering Technics Press, Edinburgh, U.K., 323–329.